

Probing Strongly Correlated Materials in Non-equilibrium: Basic Concepts and Possible Future Trends in First Principle Approaches

M. Hopjan and C. Verdozzi

Abstract Time-resolved spectroscopy has an emerging role among modern material-characterization techniques. Two powerful theoretical formalisms for systems out of equilibrium (and thus for time-resolved spectroscopy) are Non-Equilibrium Green's Functions (NEGF) and Time-Dependent Density Functional Theory (TDDFT). In this chapter, we offer a perspective (with more emphasis on the NEGF) on their current capability to deal with the case of strongly correlated materials. To this end, the NEGF technique is briefly presented, and its use in time-resolved spectroscopy highlighted. We then show how a linear response description is recovered from NEGF real-time dynamics. This is followed by a review of a recent ab initio NEGF treatment and by a short introduction to TDDFT. With these background notions, we turn to the problem of describing strong correlation effects by NEGF and TDDFT. This is done in terms of model Hamiltonians: using simple lattice systems as benchmarks, we illustrate to what extent NEGF and TDDFT can presently describe complex materials out of equilibrium and with strong electronic correlations. Finally, an outlook is given on future trends in NEGF and TDDFT research of interest to time-resolved spectroscopy.

Keywords Time-dependent spectroscopy • Strongly correlated systems • ab-initio real-time dynamics • Non-equilibrium green's functions • TDDFT • Kadanoff–baym equations • Many-body perturbation theory • Exchange correlation potential • Self-energy

M. Hopjan (✉)

Division of Mathematical Physics, Lund University, Box 118, 22100 Lund, Sweden
e-mail: miroslav.hopjan@teorfys.lu.se

C. Verdozzi

Division of Mathematical Physics and ETSF, Lund University, Box 118, 22100 Lund, Sweden
e-mail: claudio.verdozzi@teorfys.lu.se

Contents

1	Time-Resolved Spectroscopy and the Case of Strongly Correlated Materials	348
2	Plan of This Chapter	350
3	Time-Dependent Spectroscopies in General and NEGF	351
4	General Aspects of Kadanoff–Baym Formalism	355
5	Linear Response via the KBE	364
6	A Recent Ab Initio Application of the KBE	366
7	Learning from Models	369
8	DFT and TDDFT (in the Lattice Version)	371
9	Strongly Correlated Materials Out of Equilibrium: KBE or TDDFT?	374
10	Conclusion and Outlook	378
	References	380

1 Time-Resolved Spectroscopy and the Case of Strongly Correlated Materials

Exploring and exploiting the properties of matter is an activity as old as mankind itself. Indeed, it can be easily argued that the development of civilization(s) has crucially depended on finding (also by chance) novel ways to deal with matter in different forms. In a modern perspective, such activities are broadly referred to as materials science.

Progress in materials science has always been driven by defining experimental discoveries: notable examples across history are glass, bronze, steel, plastic, semiconductors, and, very recently, graphene, to name but a few. On the theoretical side, a crucial advance was the recognition that many materials properties can be understood, predicted, or even manipulated by taking into account the atomistic nature of matter. A subsequent milestone in the theoretical development was the advent of quantum mechanics. The latter provides a description of matter at the microscopic, quantum level, thus radically changing the way we investigate materials properties. Nowadays, well established and traditional subfields of materials science, such as, e.g., metallurgy, tribology, catalysis, and energy storage, all benefit greatly from the conceptual backbone provided by quantum mechanics. This also holds for the spectroscopical characterization of materials, the central topic of this book.

From the theoretical point of view, what is definitely needed in today’s materials science is an accurate (and preferably predictive) quantitative description of materials properties under a vast range of external conditions and operating regimes. There are several reasons why this is not easy to accomplish. To mention a few, the material of interest often has a complex crystal or magnetic structure (sometimes with controlled or random inhomogeneities, i.e., long range order may be missing), and this requires one to consider large structural units, with very many atoms, thus rendering numerical simulations very expensive, if not prohibitive.

In other cases, the functional property of interest requires one to consider several length scales and timescales together, an extremely challenging situation to theoretical

treatments. Furthermore, novel properties often result from materials where the role of interactions among electrons and between electrons and lattice vibrations are non-negligible. Here, an accurate quantitative description of many-body effects is mandatory (solving this problem in general is one of the great challenges of current condensed matter research) to describe spectroscopy experiments.

Finally, describing and predicting the behavior of materials out of equilibrium (i.e., in their actual operating regime) is considerably more complicated than in the equilibrium case; for example, the presence of time-varying external fields removes translational time invariance, adding considerable complexity to the theoretical description.

One of the most versatile theories to describe materials at the microscopic level is Density-Functional Theory (DFT) in the Kohn–Sham (KS) formulation. In principle exact (in practice, approximate exchange-correlation (XC) potentials need to be used), this approach provides a good account of several basic properties, e.g., inter-atomic distances, cohesive energies, structural phase transitions, and band-structure dispersion, often attaining quantitative agreement with experiment. However, for materials with strong correlation effects among the electrons, success is considerably more limited (we mention in passing another typical problem of KS band-structure calculations, namely the band gap in semiconductors and insulators is considerably underestimated with respect to its experimental value). As a result, a great deal of current theoretical developments in *ab initio* methods has to do with how to overcome these (and other) shortcomings of the available DFT treatments.

This is especially important to describe excited states and the spectroscopical behavior of materials, which are the main subjects of this book. A common denominator of Chaps. 1–8 of the book is a discussion of the currently available *ab initio* approaches that can be used in spectroscopy, e.g., for optical and photo-emission spectra. Different avenues are discussed, such as novel functionals, the extension of DFT to the time-dependent case with Time-Dependent Density Functional Theory (TDDFT), and many-body approaches based on propagator methods. A second, transversal theme in the book is how to deal with materials where correlations among electrons are important, if not pivotal, for a correct interpretation of the spectroscopic data.

For DFT-based approaches, a central open issue is how to go beyond current approximations for the XC potential (see, e.g., the contributions by Kronik and Kümmel, Dabo et al., Isseroff-Bendavid and Carter, and Şaşıoğlu et al. in this book). As shown in the chapter by Pastore et al. in this book, progress in this direction is key to a realistic description of complex functional materials. Another relevant issue in DFT and TDDFT approaches is how to treat excited states; in this case, it is important, at the linear response level, to devise improved exchange-correlation kernels in TDDFT susceptibilities, instead of solving the full many-body Bethe–Salpeter equation (see, e.g., the chapter by Sharma et al. in this book for excitonic effects in optical absorption spectra).

On the other hand, for *ab initio* many-body approaches based on perturbative schemes, a central role is played by the GW approximation (see, e.g., the contributions by Bruneval and Gatti, Isseroff-Bendavid and Carter, Şaşıoğlu et al., and

Kronik and Kümmel) which, with its wide range of applicability, currently is in many respects the method of choice to deal with complex materials. The screened exchange of the GW approximation cures several shortcomings of DFT treatments based on local and semi-local potentials, but is unable to describe correctly local correlations in strongly correlated systems. For this latter case, great improvements have been obtained in terms of non-perturbative or embedding schemes, as discussed in detail in the chapters by Biermann and by Isseroff-Bendavid and Carter in this book. Important aspects of the physics of strongly correlated systems, e.g., metal-insulator transitions due to electron correlations, or magnetic order and spin excitations, can also be addressed successfully (for this latter aspect, see also the chapter by Şaşıoğlu et al. in this book).

In Sects. 1–8, spectroscopic techniques and materials properties are primarily discussed in the frequency domain. This is very suitable for the linear response regime, where quantities such as correlation functions, spectral functions, absorption coefficients, etc., yield a wealth of information about the near-equilibrium properties of a system. And yet, spectroscopical information about excited states can also be directly obtained by performing experiments in the time domain. This is, for example, the case of the so-called pump-and-probe time-resolved spectroscopies which, with ultrafast probes, aim to reveal directly features from highly excited states in the electron/hole dynamics in a material. From the theoretical point of view, describing such experiments requires the use of non-equilibrium, time-dependent approaches, and an inherent key aspect is how to take properly into account the correlated electron dynamics. Addressing this issue, as relevant to time-dependent spectroscopies, is the main aim of this chapter.

2 Plan of This Chapter

For our discussion of time-dependent spectroscopies, we need to introduce several concepts, and to compare and apply different methodologies to several different physical systems. It may thus be useful for the reader to rely on the present section as a sort of guidance through the different parts of the chapter.

In what follows, we will consider two methods which have great potential to describe time-resolved spectroscopy at the *ab initio* level: the non-equilibrium Green's function (NEGF) technique (in the following, we also refer to it as the Kadanoff–Baym equations (KBE), see below) and TDDFT. Due to the expanding capability of computers, full numerical solutions of the KBE are starting to appear although, primarily, for model systems. Different is the case of TDDFT, which has been extensively applied to materials characterization (mostly in a linear response framework; studies of the real-time dynamics of materials via *ab-initio* TDDFT still are less common). The performance of both NEGF and TDDFT relies on an accurate treatment of a pivotal ingredient (the self-energy for the NEGF and the XC potential for TDDFT), and good progress has been made in dealing with a broad range of systems; however, for materials out of equilibrium (e.g., in time-resolved

spectroscopy experiments), *ab initio* TDDFT and NEGF treatments of strong electronic correlations currently remain rather inadequate. In this situation, it may also be useful to analyze results from simple, strongly correlated model systems, to gain qualitative insight into the problem. This is the perspective adopted here, where in our discussion we interchangeably make use of notation and concepts from the general *ab initio* case and/or from model-system treatments.

The emphasis of our presentation will be different for the two methods: we will devote more space to the principles of the NEGF technique (which has not been considered in the rest of the volume) than to TDDFT (for a thorough discussion see the contribution by Sharma et al.). However, in the final part of this chapter, the results from both methods for simple models will be discussed on an equal footing to contrast different qualitative aspects of electronic correlations and how successfully they are currently dealt with within NEGF and TDDFT approaches.

In more detail, the rest of this chapter is organized as follows. (i) We start with a short introduction of time-resolved spectroscopy (Sect. 3) to indicate the quantities of interest within the NEGF approach. (ii) We then present the basic notions of the NEGF-KBE formalism in Sect. 4. (iii) In Sect. 5, the linear response regime is discussed from the NEGF perspective (this shows the potential advantage of solving the KBE even in the linear-response regime, thus avoiding the direct solution of a Bethe–Salpeter equation). (iv) We briefly review a recent *ab initio* study in Sect. 6 to show the state-of-the-art of NEGF implementations for real materials. (v) We then resort to model (Hubbard-type) Hamiltonians to address strong correlation effects out of equilibrium (Sect. 7). (vi) This is followed by a short review of lattice (TD)DFT, within and beyond the linear response regime in Sect. 8, to deal with strongly correlated lattice models in Sect. 9. (vii) We use recent benchmark results, which illustrate the importance of both non-perturbative and non-adiabatic effects in real-time dynamics, to contrast the respective advantages and current limitations in TDDFT and/or NEGF formulations (Sect. 9) when electronic correlations are important. (viii) This is followed by our conclusions and outlook in Sect. 10.

3 Time-Dependent Spectroscopies in General and NEGF

Time-resolved spectroscopy is the name broadly given to a set of experimental tools that allow for the measurement of time-resolved quantities in photo-excited systems. Common examples are time-resolved infrared or fluorescence spectroscopies and studies of photo-induced chemical reactions, relaxation processes of excited states in metals, semiconductors, and complex materials. Electron relaxation driven by electron–electron and electron–lattice scattering has been observed for quite some time in experiments from ordinary metals and semiconductors. However, in many other systems, the electron dynamics may be much faster, and one needs a time resolution on the femtosecond or even attosecond scale. Here, we wish to illustrate briefly some theoretical concepts necessary for a description of these

experimental techniques in terms of NEGF. Our concise presentation in this section is based on [1–3]. As, additional, general reference sources, we also mention the papers [4, 5] and the reviews in [6, 7].

Femtosecond resolution can be achieved by ultrafast optics and a frequently used technique is the so-called pump-probe setup. The pump pulse brings a sample out of equilibrium, and the excited states subsequently start to decay. During this transient period, a very short probe pulse is used to take a snapshot of the sample. The time delay t_p between the pump pulse and probe is usually well controlled.¹ For higher time resolution, shorter and more intensive laser pulses are needed. The most advanced techniques generate sub-10 fs pulses in the visible and infrared spectrum.

Nowadays, attosecond resolution is generated by controlled light fields, and sub-femtosecond pulses (electron or X-rays) can be reached. The pulses can either be used as pump or as probe; therefore, there is no restriction due to femtosecond light-envelopes as for the case of ultrafast optics [7]. Attosecond pump-probe experiments are also promising candidates for future better resolution of the electron–lattice interaction processes.

Quantities from ultrafast spectroscopy cannot be calculated by a straightforward use of the linear-response formalism in frequency space, essentially for two reasons.

1. First, the processes are inherently time-dependent and this can be accounted for by the two-time, time-dependent Green’s function $G^<(t_1, \mathbf{r}_1, t_2, \mathbf{r}_2)$. This quantity is the central concept of the NEGF technique, and is discussed in good detail in the next section. Here, suffice it to say that the Green’s function contains information about excitations in the sample, and is related to the density matrix via

$$\rho(t_1, \mathbf{r}_1, \mathbf{r}_2) = -iG^<(t_1, \mathbf{r}_1, t_1, \mathbf{r}_2), \quad (1)$$

for real time t_1 . The one-time density matrix does not treat the energy as an independent variable, whereas the two-time Green’s function does. The two-time structure is crucial for the description of the inherent time-dependence. A very important two-time quantity is defined as

$$A(1, 2) = i[G^>(1, 2) - G^<(1, 2)], \quad (2)$$

which is a combination of the lesser and greater Green’s functions (see the next section). In equilibrium, A becomes the spectral function. In the Wigner representation, where one has $t = t_1 - t_2$ and $T = \frac{t_1+t_2}{2}$ and the dependence on t is transferred to the energy space ω , A might be referred to as “ T -time dependent

¹ A good control is highly desirable, since the energy and tuning of the perturbing fields also affect the spectrum characteristics. For example, in time-resolved two-photon photoemission spectroscopy, the energy shift between the photon energies of the pump and probe permits one to relate peaks in the spectrum with initial and/or intermediate states [6].

spectral function” $A(T, \omega, \mathbf{r}_1, \mathbf{r}_2)$. In equilibrium, or in the steady state, A becomes independent of T , and depends only on ω . A time-dependent pole structure in the “spectral function” gives us the information about the addition/removal energies.

2. Second, we are dealing with processes that involve strong interactions between the probe and the system. Examples are (strongly) nonlinear optics, attosecond dynamics, ionization yields, high-harmonic generation, and quantum control of electronic/ionic processes. In principle the NEGF technique is a tool for computing the effect of correlations beyond linear response, since the external fields (both pump and probe) are treated non-perturbatively. The complex dynamics of the pump pulse can somehow expediently be avoided by making use of a non-equilibrium initial density matrix $\rho(t) = -iG^<(t, t)$ or by performing an interaction quench [3, 8]. This second prescription attempts to imitate the initial condition of the excited system and thus one can focus only on the relaxation and interaction with the probe (however, in this way only a qualitative picture of the effect of the pump can be expected). Yet, we wish to emphasize that the NEGF approach (as presented in Sect. 4) can describe in full generality the dynamics induced by both the pump and the probe, starting from the true equilibrium state.

In femtosecond and attosecond spectroscopy there are two main experimental techniques, Time-Resolved Optical Spectroscopy and Time-Resolved Photoemission Spectroscopy. They both make use of the pump-probe setup, while differing in the probe technique. We now wish to illustrate where and how connections with the NEGF appear in the theoretical formulation for these two spectroscopies. Our discussion and notation closely follow [1–3].

In optical spectroscopy, after the medium is driven out of equilibrium by the pump pulse, one studies the dynamical response to the light probe. The probe field is supposed to be weak, and we use linear response to investigate the change δj of a current $j_\alpha(\mathbf{r}, t)$ driven by a variation of the probe field $\delta E_\beta(\mathbf{r}, t)$ (α, β label space-components, and summation is implied for repeated indexes):

$$\delta j_\alpha(\mathbf{r}, t) = \int_{-\infty}^t dt' \sigma_{\alpha\beta}(t, t') \delta E_\beta(\mathbf{r}, t'). \quad (3)$$

The optical conductivity $\sigma_{\alpha\beta}(t, t')$ is defined via the susceptibility response function $\chi_{\alpha\beta}(t, \bar{t})$ as

$$\sigma_{\alpha\beta}(t, t') = -c \int_{t'}^{\infty} d\bar{t} \chi_{\alpha\beta}(t, \bar{t}), \quad (4)$$

consistent with causality constraints [1]. For the susceptibility response function, the following relation holds:

$$\chi_{\alpha\beta}(t, t') = \frac{\delta \langle j_\alpha(t) \rangle}{\delta A_\beta(t')} = \sum_{\mathbf{k}\sigma} \frac{i}{V} \left(\frac{\delta v_{\alpha\mathbf{k}\sigma}(t)}{\delta A_\beta(t')} G_{\mathbf{k}\sigma}^<(t, t) + v_{\alpha\mathbf{k}\sigma}(t) \frac{\delta G_{\mathbf{k}\sigma}^<(t, t)}{\delta A_\beta(t')} \right), \quad (5)$$

where $A_\beta(t)$ denotes the vector potential component ($\mathbf{E} = -\frac{1}{c} \frac{\partial \mathbf{A}}{\partial t}$), $G_{\mathbf{k}\sigma}^<(t, t)$ the lesser Green's function in the \mathbf{k} -representation (see the next section), and the electron group velocity $v_{\alpha\mathbf{k}\sigma}(t)$ accounts for the details of the band structure and for the presence of the electric field. The expression for χ (see [1, 3] for a full derivation) clearly shows the connection between the NEGF and the optical conductivity through the susceptibility function.

In photoemission spectroscopy, the pump pulse excites the system to a general non-equilibrium state and then, after a delay t_p , a probe pulse of specific shape and finite duration is used to induce an emission of electrons from the sample. The photoemission signal intensity as a function of t_p is related to the NEGF. The time-resolved photoemission signal is defined as the total number of electrons that are emitted per solid angle $d\Omega_{\hat{\mathbf{k}}_e}$ and energy interval dE [2, 3]

$$I(\hat{\mathbf{k}}_e, E; \mathbf{q}, t_p) = \frac{dN(\hat{\mathbf{k}}_e, E; \mathbf{q}, t_p)}{d\Omega_{\hat{\mathbf{k}}_e} dE}, \quad (6)$$

where $\hat{\mathbf{k}}_e$ is the direction vector of the electron momentum $\mathbf{k}_e = \hat{\mathbf{k}}_e k_e$, and \mathbf{q} is a specific wave vector of the probe pulse. The photoemission caused by the pump pulse is not considered because the pump radiation is chosen such that its photons do not have sufficient energy to overcome the work function Φ of the sample [9].

The photoemission is described by a model which consists of three parts (we use standard second quantization notation; for more detailed definitions see the next section): $\hat{H} = \hat{H}_{\text{solid}}(t) + \hat{H}_{\text{free}} + \hat{H}_{\text{coupl.}}(t)$. \hat{H}_{solid} describes the electrons in the bulk (see, e.g., (10)), while $\hat{H}_{\text{free}} = \sum_{\mathbf{k}_e\sigma} (E + \Phi) \hat{\phi}_{\mathbf{k}_e\sigma}^\dagger \hat{\phi}_{\mathbf{k}_e\sigma}$ describes electrons emitted to the vacuum with asymptotic state with momentum \mathbf{k}_e . The last part $\hat{H}_{\text{coupl.}}$ connects the free-electron states with momentum \mathbf{k}_e to the bulk ones with momentum \mathbf{k} via the absorption of a photon with momentum \mathbf{q} :

$$\hat{H}_{\text{coupl.}}(t) = S(t - t_p) \sum_{\mathbf{k}, \mathbf{k}_e, \sigma} M(\mathbf{k}, \mathbf{q}; \mathbf{k}_e) e^{i\omega_q t} \hat{\phi}_{\mathbf{k}_e\sigma}^\dagger \hat{\psi}_{\mathbf{k}\sigma} + \text{h.c.}, \quad (7)$$

where $\omega_q = cq$ and the transition matrix M is expressed in terms of the electromagnetic coupling $\mathbf{A} \cdot \mathbf{p}$. The function $S(\tau)$ describes an envelope function of the probe pulse centered around $\tau = 0$.

The relation between the photoemission signal and the NEGF has a simple form in the so-called sudden approximation, where there is no direct interaction between the bulk and free emitted electrons. Otherwise, in a more general and complete treatment, a three-current correlation function is needed [4, 5], which can be evaluated within the NEGF scheme. In the sudden approximation, where the probe is considered as a weak perturbation, the intensity takes the form [2, 3]

$$I(\hat{\mathbf{k}}_e, E; \mathbf{q}, t_p) = \sum_{\mathbf{k}, \sigma} \delta_{\mathbf{k}_{\parallel} + \mathbf{q}_{\parallel}, \mathbf{k}_{e\parallel}} \mathcal{I}_{\mathbf{k}, \sigma}(E - \omega_q - \Phi; t_p), \quad (8)$$

$$\mathcal{I}_{\mathbf{k},\sigma}(\Omega; t_p) = -i \int dt \int dt' S(t) S(t') e^{i\Omega(t'-t)} G_{\mathbf{k}\sigma}^<(t + t_p, t' + t_p). \quad (9)$$

In Eckstein and Kollar [2], in deriving (8) and (9), two additional assumptions were made: (a) one is dealing with a translationally invariant system, i.e., $G_{\mathbf{k}\sigma}^<(t, t') = G_{\mathbf{k}\sigma, \mathbf{k}\sigma}^<(t, t')$ and (b) a constant form for $M(\mathbf{k}, \mathbf{q}; \mathbf{k}_e) = M\delta_{\mathbf{k}||+\mathbf{q}||, \mathbf{k}_e||}$ is considered. A more involved expression holds for the non-homogeneous case, and when dispersion in the transition matrix element is kept. However, these more technical issues are not especially relevant for our main deliberations here, which were to illustrate a direct connection between time-resolved photoemission signal and the NEGF.

To summarize, for a full description of the pump-probe technique it is necessary to go beyond linear response. In full generality, the NEGF technique is able to take into account the pump and probe pulses (the external fields) non-perturbatively. As we will see in Sect. 4, this requires a double-time-integration of the equation of motion for the two-time, non-equilibrium Green's function (i.e., the KBE). In the past, this was basically impossible, because there was insufficient computational power, and thus only primarily linear response calculations. However, once the full solution of the KBE becomes tractable with computers, the near-equilibrium properties can be accessed via NEGF. The connection between NEGF and linear response theory helps to solve the Bethe–Salpeter equation very effectively, even for advanced kernels. The reason is that a simple kernel in the KBE is translated into a very complicated kernel in the Bethe–Salpeter equation [10, 11]. These points are discussed in more detail in the following sections.

4 General Aspects of Kadanoff–Baym Formalism

We wish now to briefly present the main features of NEGF (also referred to as Kadanoff–Baym or Keldysh formalism). Motivated by pump-probe experiments (see Sect. 3) we are interested in the evolution of a general non-equilibrium system after (pump) or during (probe) the influence of external fields. Such a system is described by the general Hamiltonian (in atomic units $\hbar = m = e = 1$)

$$\begin{aligned} \hat{H}(t) &= \int d\mathbf{x} \hat{\psi}^\dagger(\mathbf{x}) \left(\frac{[-i\nabla + A(\mathbf{x}, t)]^2}{2} + \Phi(\mathbf{x}, t) - \mu \right) \hat{\psi}(\mathbf{x}) \\ &+ \iint d\mathbf{x}_1 d\mathbf{x}_2 \hat{\psi}^\dagger(\mathbf{x}_1) \hat{\psi}^\dagger(\mathbf{x}_2) \hat{V}(\mathbf{x}_1, \mathbf{x}_2) \hat{\psi}(\mathbf{x}_2) \hat{\psi}(\mathbf{x}_1) \\ &+ \int d\mathbf{x} \hat{V}_{\text{el.-ph.}}(\mathbf{x}) \hat{\psi}^\dagger(\mathbf{x}) \hat{\psi}(\mathbf{x}) \hat{\phi}(\mathbf{x}) \\ &+ \int d\mathbf{x} \left(\frac{1}{2} \hat{\phi}^2(\mathbf{x}) + \frac{1}{2} (\nabla \hat{\phi})^2(\mathbf{x}) \right) \\ &= \hat{H}_0 + \hat{H}_{\text{inter.}} + \hat{H}_{\text{ext.}}(t) + \hat{H}_{\text{el.-ph.}} + \hat{H}_{\text{ph.}}, \end{aligned} \quad (10)$$

where μ is chemical potential, $\hat{\psi}^\dagger(\mathbf{x})/\hat{\psi}(\mathbf{x})$ are creation and annihilation operators of the fermionic field which is coupled to the gauge field $(\Phi(\mathbf{x}), A(\mathbf{x}))$, and the density operator $\hat{\phi}(\mathbf{x}) \approx (\hat{b}(\mathbf{x}) + \hat{b}^\dagger(\mathbf{x}))$ represents the bosonic field for the phonons. The terms $\hat{H}_0, \hat{H}_{\text{inter.}}, \hat{H}_{\text{ext.}}$, and $\hat{H}_{\text{ph.}}$, respectively, describe Bloch electrons, the interactions among electrons (responsible for the electron–electron scattering), the external fields (responsible for the effect of the pump and probe fields during a spectroscopy experiment), and the free phononic field. The interaction between the electrons and the lattice vibration is described by the electron–phonon coupling term $\hat{H}_{\text{el.-ph.}}$ [12] (in the following, electron–lattice interactions are explicitly considered only in Sect. 6). For a macroscopic system described by the Hamiltonian of (10), a full solution for the many-body wave function cannot, in general, be obtained. In contrast, one-body or two-body quantities, such as currents or density–density correlation functions, are still of great interest, but also much easier to determine. The central quantity in the NEGF is the non-equilibrium Green’s function $G(t_1, t_2)$, from which, for example, the addition/removal spectrum, the density, and the current can be extracted. Due to the two-time dependence, the Green’s function contains a significant amount of information. However, with this complexity, computational costs for a solution are high, and represent a serious bottleneck when trying to perform ab initio simulations.

The causal Green’s function $G(1,2)$ is usually defined as

$$G(1,2) = -i\mathbf{Tr}\{\hat{\rho}\mathbf{T}\hat{\psi}(1)\hat{\psi}^\dagger(2)\}, \quad (11)$$

where $\hat{\psi}^\dagger(2)/\hat{\psi}(1)$ denotes a creation/annihilation operator in the Heisenberg picture and the symbol $1 = (t_1, r_1, \sigma_1)$ is a combined time-space-spin index. \mathbf{Tr} denotes summation over a complete basis weighted by the density matrix $\hat{\rho}$ and \mathbf{T} is a time ordering operator, which requires a generalization for non-equilibrium systems.

Instead of the causal Green’s function, we are more interested in the lesser Green’s function $G^<(1,2)$ defined for both equilibrium and non-equilibrium as

$$G^<(1,2) = i\mathbf{Tr}\{\hat{\rho}\hat{\psi}^\dagger(2)\hat{\psi}(1)\}, \quad (12)$$

now without time ordering \mathbf{T} . This is motivated by the following connection with the density matrix:

$$\begin{aligned} \rho(t, \mathbf{r}_1, \sigma_1, \mathbf{r}_2, \sigma_2) &= -iG^<(t, \mathbf{r}_1, \sigma_1, t, \mathbf{r}_2, \sigma_2) \\ &= \mathbf{Tr}\{\hat{\rho}\hat{\psi}^\dagger(t, \mathbf{r}_2, \sigma_2)\hat{\psi}(t, \mathbf{r}_1, \sigma_1)\}. \end{aligned} \quad (13)$$

In experiments, before the external fields are applied, the system is prepared in equilibrium. The initial density matrix then takes the form of the Gibbs grand canonical distribution, and the lesser Green’s function reads

$$G^<(1, 2) = i \frac{\text{Tr}\{e^{-\beta\hat{H}(t_0)}\hat{\psi}^\dagger(2)\hat{\psi}(1)\}}{\text{Tr}\{e^{-\beta\hat{H}(t_0)}\}}, \quad (14)$$

where the chemical potential μ is inside the initial Hamiltonian and the inverse temperature β are related to the initial conditions. It should be stressed at this point that the initial Hamiltonian $\hat{H}(t_0) = \hat{H}_0 + \hat{H}_{\text{int.}} + \hat{H}_{\text{el.-ph.}} + \hat{H}_{\text{ph.}}$ at time t_0 does not contain external fields, but the evolution of the operators is treated in the Heisenberg picture with respect to the full Hamiltonian $\hat{H}(t)$ where the fields are included.

If there are no external fields, the system remains in equilibrium and evolves according to $\hat{H}(t_0)$, and we end up with the usual equilibrium Green's functions, i.e., the finite temperature formalism. Moreover, if the system is in its ground state we end up with ground-state Green's functions, i.e., the zero temperature formalism.

Historically, the development of Green's function theory for non-equilibrium systems was preceded by ground state theories at zero temperature (Feynman [13], Dyson [14], Wick [15]) and the equilibrium theories for finite temperature (Matsubara [16]). Both of them account for interactions, while being conceptually distinct in important ways. The theory for zero temperature introduces an artificial adiabatic interaction switching procedure, and the finite temperature theory uses the similarity of the grand-canonical and evolution operator. As a consequence, the Feynman theory covers evolution in real-time whereas Matsubara theory covers evolution within a segment $[t_0, t_0 - i\beta]$ using imaginary time (see the imaginary-time and real-time contours in Fig. 1).

The question is then how to incorporate time-dependent perturbations $\hat{H}_{\text{ext.}}(t)$. The two theories mentioned cannot be directly generalized. In the zero-temperature theory, the adiabatic procedure fails when the external field is applied. Briefly, one cannot easily connect states in the past and future as in the ground-state case. In the finite temperature theory, the evolution in imaginary time obviously starts to be an issue because of the real-time dependence of the external fields. The problem of how to perform time-evolution from initial equilibrium can be solved by introducing a so-called Schwinger–Keldysh contour, depicted in Fig. 1. The idea was pioneered by Schwinger [17] followed by Kadanoff–Baym [18], popularized by Konstantinov and Perel [19] and Keldysh [20], and in a clear way was reviewed by Danielewicz [21].

The concept of Schwinger–Keldysh contour: In the zero-temperature theory, the mean value of an operator \hat{O} averaged over the interacting ground state $|\psi_0^t\rangle$ is given by $\langle\psi_0^t|\hat{O}(t)|\psi_0^t\rangle$. The latter expression can be formally written as a time-evolution with adiabatically switched on/off interactions $\frac{\langle\psi_i|S(\infty,0)\hat{O}(t)S(0,-\infty)|\psi_i\rangle}{\langle\psi_i|S(\infty,-\infty)|\psi_i\rangle}$ where $|\psi_i\rangle$ is the initial state in the infinite past. At time $t = 0$ we reach the fully interacting system. The time evolution is without the external force, and thus

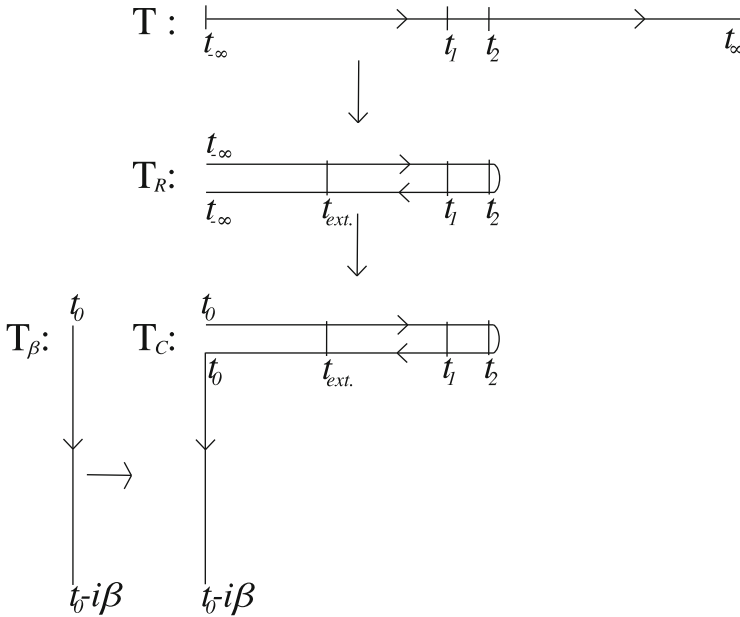


Fig. 1 The real-time contour (*top*), the Round trip contour (*center*) given by distortion of the real-time contour, the imaginary-time contour $t \in [t_0, t_0 - i\beta]$ (*bottom left*), and the Schwinger-Keldysh contour (*bottom right*). Each contour has its own time-ordering, according to the inherent contour orientation (the *arrows* on the contours). Interactions can be taken into account within each of these contours. At time $t_{ext.}$ we switch on the external fields and the system is driven out of equilibrium; this can be implemented in the upper branch of the Round trip contour. On the lower branch of the Round trip contour we switch off the fields and end up with the initial equilibrium state. In the Schwinger-Keldysh contour there is no necessity for an adiabatic interaction switching because interactions can already be included within the vertical imaginary track

$S(t', t) = \mathbf{T}e^{-i \int_t^{t'} \hat{H}_{pert.}(\tau) d\tau}$, where the perturbed Hamiltonian $\hat{H}_{pert.}(t) = \hat{H}_{inter.}(t)$ is in the interaction picture with respect to \hat{H}_0 . The operator \mathbf{T} orders times as shown by the arrow in the real-time contour in Fig. 1). We use the fact that, in the zero temperature formalism, there exists a simple connection between the initial state $|\psi_i\rangle$ and the final state $|\psi_f\rangle$ in the infinite future, i.e., $|\psi_f\rangle = \frac{|\psi_i\rangle}{\langle \psi_i | S(\infty, -\infty) | \psi_i \rangle}$. Going from the Heisenberg's picture $\hat{O}(t)$ to the Dirac's interaction picture \hat{O}_t , one can rewrite the average as $\frac{\langle \psi_i | S(\infty, t) \hat{O}_t S(t, -\infty) | \psi_i \rangle}{\langle \psi_i | S(\infty, -\infty) | \psi_i \rangle}$. The time evolution of any observable $O(t)$, making use of \mathbf{T} , can then simply be written as $\frac{\langle \psi_i | \mathbf{T}(\hat{O}_t S(\infty, -\infty)) | \psi_i \rangle}{\langle \psi_i | S(\infty, -\infty) | \psi_i \rangle}$. We should mention here that above idea is rigorously proved by the Gell-Mann-Low theorem [22].

If the system undergoes a time-evolution under the influence of an external field, then the system is no longer in equilibrium, and thus it ends up in a final state which is not connected to the initial one. The connection $|\psi_f\rangle = \frac{|\psi_i\rangle}{\langle\psi_i|S(\infty, -\infty)|\psi_i\rangle}$ no longer applies; the real-time contour is not suitable. In order to get the average value over the initial states, we do the time evolution according the Round trip contour; see Fig. 1. It is obvious that in this contour the final state is the same as the initial one, because we are going back and forth between time $t_0 = -\infty$ and time of interest t . The evolution of the operator $\hat{O}(t)$ can thus be simply written as $\frac{\langle\psi_i|\mathbf{T}_R(\hat{O}, S(-\infty, -\infty))|\psi_i\rangle}{\langle\psi_i|S(-\infty, -\infty)|\psi_i\rangle}$. The time \mathbf{T}_R ordering corresponds to the Round trip contour. In this way, we get the same formal expression $\langle\psi_i|\dots|\psi_i\rangle$ for both the zero temperature and the non-equilibrium theory.

Why do we also include the vertical track? In general the initial state can be a thermal-equilibrium interacting state. Then we handle this state in the spirit of Matsubara theory by adding the vertical track of the Matsubara formalism. In this way we do not need to switch on/off adiabatically the interaction in the Round trip contour and thus the evolution does not need to start in the infinite past.

The Schwinger–Keldysh contour γ thus consists of three branches. The evolution in the horizontal branches corresponds to propagating in real time from t_0 to the times of interest (t_1 and t_2), then going backwards to the initial time t_0 . This can be summarized as

$$\hat{\psi}^\dagger(2)\hat{\psi}(1) = U(t_0, t_2)\hat{\psi}^\dagger(\mathbf{r}_2)U(t_2, t_1)\hat{\psi}(\mathbf{r}_1)U(t_1, t_0), \quad (15)$$

where $\hat{\psi}^\dagger/\hat{\psi}$ are now in the Schrödinger picture (the time evolution is in the presence of the external force and this is accounted for by the operator $U(t', t) = \mathbf{T}_R e^{-i \int_t^{t'} (\hat{H}_0 + \hat{H}_{\text{pert.}}(\tau)) d\tau}$ with perturbed Hamiltonian $\hat{H}_{\text{pert.}}(t) = (\hat{H}_{\text{inter.}} + \hat{H}_{\text{ext.}})(t)$; \mathbf{T}_R orders times as shown by the arrow in Fig. 1).

The third part of the contour comes from finite temperature theory. The equilibrium statistical operator is

$$\hat{\rho} = \frac{e^{-\beta\hat{H}(t_0)}}{\mathbf{Tr}\{e^{-\beta\hat{H}(t_0)}\}} \quad (16)$$

and includes the effect of the interactions in the initial equilibrium state (initial correlations). Taking this into account leads to the lesser non-equilibrium Green's function

$$G^<(1, 2) = i \frac{\mathbf{Tr}\{U(t_0 - i\beta, t_0)U(t_0, t_2)\hat{\psi}^\dagger(\mathbf{r}_2)U(t_2, t_1)\hat{\psi}(\mathbf{r}_1)U(t_1, t_0)\}}{\mathbf{Tr}\{U(t_0 - i\beta, t_0)U(t_0, t_0)\}}. \quad (17)$$

where the time evolution in the vertical branch is indicated by $\mathcal{U}(t', t)$ (the time evolution is without the external force and this is accounted for by the operator $\mathcal{U}(t', t) = \mathbf{T}_\beta e^{-i \int_t^{t'} (\hat{H}_0 + \hat{H}_{\text{pert.}}(\tau)) d\tau}$ with perturbed Hamiltonian $\hat{H}_{\text{pert.}}(t) = \hat{H}_{\text{inter.}}(t)$; \mathbf{T}_β orders times as shown by the arrow in the vertical track in Fig. 1).

Returning to the causal Green's function, we need to change our naive definition in (11), since it contains the time-ordering operator \mathbf{T} inspired by Feynman's theory. For the Schwinger–Keldysh contour, we need to generalize (11). All evolution operators (either U or \mathcal{U}) can be formally joined into one time-ordered exponential as

$$G(1, 2) = -i \frac{\text{Tr} \left\{ \mathbf{T}_C e^{-i \int_\gamma \hat{H}(\tau) d\tau} \hat{\psi}_{t_1}(\mathbf{r}_1) \hat{\psi}_{t_2}^\dagger(\mathbf{r}_2) \right\}}{\text{Tr} \left\{ \mathbf{T}_C e^{-i \int_\gamma \hat{H}(\tau) d\tau} \right\}}. \quad (18)$$

We stress here that $\hat{\psi}_{t_1}/\hat{\psi}_{t_2}^\dagger$ are not in Heisenberg picture. Here, t_1 and t_2 are on the Schwinger–Keldysh contour and \mathbf{T}_C order times on the contour; for example, $t_1 <_C t_2$ means that going from t_0 to $t_0 - i\beta$ one meets t_1 earlier than t_2 [23, 24]. For such a definition of G the structure of the equilibrium formulation is preserved, and we can apply Wick's theorem, many-body perturbation schemes, the Dyson's equation, the renormalization procedure, etc. The Dyson equation for the causal Green's function

$$G(1, 2) = G_0(1, 2) + \int_\gamma G_0(1, 3) \Sigma(3, 4) G(4, 2) d3 d4 \quad (19)$$

defines the self-energy $\Sigma = G_0^{-1} - G^{-1}$, where the integration is over the Schwinger–Keldysh contour γ with time-ordering fixed by \mathbf{T}_C . The Dyson integral equation can be converted to its differential form

$$G_0(1, 2)^{-1} G(1, 2) = \delta(12) + \int_\gamma \Sigma(1, 4) G(4, 2) d4, \quad (20)$$

more explicitly

$$\left(i \frac{\partial}{\partial t_1} - H_0 - u(1) \right) G(1, 2) = \delta(12) + \int_\gamma \Sigma(1, 4) G(4, 2) d4, \quad (21)$$

which is usually solved by propagation from the initial state given by the solution of the equation in imaginary time. The external fields are denoted by $u(1)$ and are treated non-perturbatively. The self-energy, on the other hand, accounts for the

effects of the electron–electron and the phonon–electron interaction and is usually approximated.

Such approximations for Σ are usually constructed via a selection of terms from a perturbation series for $\Sigma[G_0]$ in terms of the free propagator G_0 . This is followed by a renormalization procedure where, in the so-called skeleton diagrams, the free propagators are replaced by the full Green’s function. This gives a final, self-consistent approximation $\Sigma[G]$.

Another way to access an approximate $\Sigma[G]$ makes use of the equation of motion for G :

$$\left(i \frac{\partial}{\partial t_1} - H_0 - u(1)\right)G(1, 2) = \delta(12) - i \int_{\gamma} V(1^+, 3)G_2(1, 3, 3^+, 2)d3, \quad (22)$$

where the two-particle Green’s function G_2 couples to the one-particle G and where 3^+ is infinitesimally later than 3 on the contour. This method is referred to as the functional derivative method (see, e.g., the monograph by Kadanoff and Baym [18]). In this approach, the self-energy is viewed as a decoupling scheme for the two-particle Green’s function $G_2 \approx \langle \hat{\psi}^\dagger \hat{\psi}^\dagger \hat{\psi} \hat{\psi} \rangle$ in the Schwinger–Martin [17] hierarchy, in terms of G and the interaction V . The way to decouple G_2 is not obvious a priori and can be done in different ways.

One obvious possibility is to use for the non-equilibrium case the approximations already known from equilibrium. Among these, very common ones are the self-consistent Hartree, Hartree–Fock, 2nd-Born, GW, and T -matrix approximations. These perturbative schemes conserve macroscopic quantities such as the number of particles, momentum, angular momentum, and energy [23, 25, 26], which are very desirable (in fact, crucial) properties in out-of-equilibrium treatments. Non-conserving approximations are also common, in cases where condensation occurs, for example in superconductors, where the decoupling is called anomalous [27].

It was shown that conserving approximations could be derived from a potential Φ , and for this reason, they are also called Φ -derivable approximations. The first and second functional derivatives of Φ are the self-energy Σ and the kernel Γ , respectively, which will be discussed later in Sect. 5 in connection to the Bethe–Salpeter equations; see Fig. 2. The T -matrix ladder approximation is usually used for systems with short-range interactions (or in the dilute limit), while, in the GW approximation (which takes into account the screening effects in solids and is largely used, e.g., for semiconductors), the adopted point of view is that a first-order expansion in the screened interaction should be more successful than one in terms of the bare Coulomb interaction.

Numerical integration of the Kadanoff–Baym equations: We sketch here the procedure to integrate numerically the KBE. To get G at all times t_1, t_2 , we consider










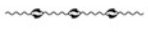

	a	b	c	d
Φ				
$\frac{\delta\Phi}{\delta G}$				
$\frac{\delta^2\Phi}{\delta G^2}$	$\{$			

Fig. 2 Examples of diagrams for the generating potential $\Phi[V, G]$, the self-energy $\Sigma[V, G] = \frac{\delta\Phi}{\delta G}$, and the kernel $T[V, G] = \frac{\delta^2\Phi}{\delta G^2}$ of the Bethe–Salpeter equation

$$(i\partial_{t_1} - h(1))G(12) = \delta(12) + \int_{\gamma} \Sigma(13)G(32)d3, \tag{23}$$

$$(-i\partial_{t_2} - h(2))G(12) = \delta(12) + \int_{\gamma} G(13)\Sigma(32)d3. \tag{24}$$

The kernel Σ , for many-body approximations (MBA) based on partial summations such as those in Fig. 3, will in general be a contraction of the Green’s function with another quantity which also obeys an auxiliary Dyson equation [29]. For example, in the *T*-matrix approximation (TMA) for the particle-particle channel, the expression for the self-energy is (*V* denotes the interaction)

$$\Sigma_{\text{TMA}}(12) = \Sigma_{\text{HF}} + i \int_{\gamma} V(13)G(43)T(34)V(42)d34. \tag{25}$$

Apart from the Hartree–Fock term, Σ is expressed in terms of the *T*-matrix:

$$T(12) = \phi(12) - \int_{\gamma} \phi(13)V(34)T(42)d34. \tag{26}$$

The *T*-matrix is defined via a summation of ladder diagrams in the particle–particle channel, up to infinite order. Such diagrams are represented in the right hand column of Fig. 2 and in row c) of Fig. 3. The building block in summing these diagrams is $\phi(12) = -iG(12)G(12)$. The KBE integral equations and the equations for the self-energies are to be solved self-consistently at all times. The Keldysh quantities involved in the KBE satisfy a set of symmetries that can be used during the numerical time propagation. As an illustration, for *G* we have

$$G^{\geq}(12) = -G^{\geq}(21)^{\dagger}, \quad G^{R/A}(12) = G^{A/R}(21)^{\dagger}, \tag{27}$$

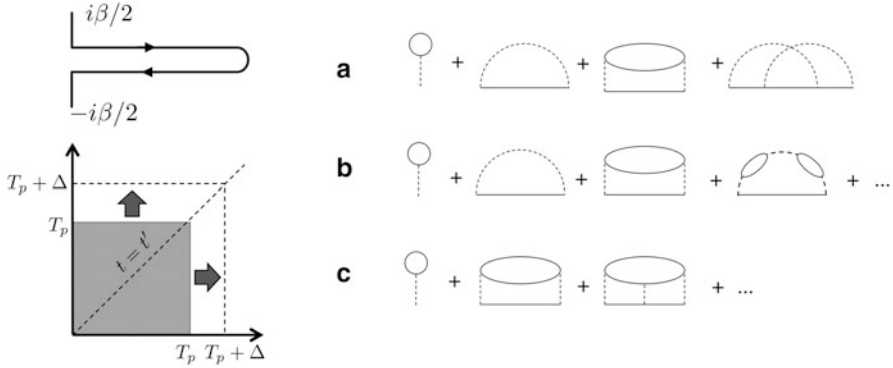


Fig. 3 *Top left:* A type of Keldysh contour [28]. *Bottom left:* Time square. *Right:* MBA via partial diagrammatic summations: (a) second Born approximation (BA); (b) GW approximation (GWA); (c) *T*-matrix approximation (TMA). Exchange TMA diagrams are not shown

and similar relations hold for Σ and other auxiliary quantities (such as T , W , etc.). Due to these symmetries, all quantities need only to be determined on the lower/upper half of the time-square (see Fig. 3), during the time expansion from T_p to $T_p + \Delta$. Since the equations involve self-consistency, predictor-corrector algorithms are employed.

One can treat Σ_{HF} , the time-local part of the self-energy, together with the non-interacting terms; that is, one defines $\mathfrak{h} = h + \Sigma_{\text{HF}}$ and thus explicitly, in the KBE, only the correlation part Σ_c appears. This can also make the time-evolution numerically more stable/accurate. For the sake of illustration, we use the symmetric contour of Fig. 3 (other contours can be used; see [28, 30] for a discussion), where, using the Langreth's rules [31], the equation for $G^<$ becomes

$$\begin{aligned}
 i\partial_{t_1} G^{\lessgtr}(t_1, t_2) &= \mathfrak{h}(t_1)G^{\lessgtr}(t_1, t_2) + I_1^{\lessgtr}(t_1, t_2), & (28) \\
 I_1^{\lessgtr}(t_1, t_2) &= \int_0^{t_1} d\bar{t} [\Sigma_c^R(t_1, \bar{t})G^{\lessgtr}(\bar{t}, t_2) + \Sigma_c^{\lessgtr}(t_1, \bar{t})G^A(\bar{t}, t_2)] \\
 &+ \frac{1}{i} \int_0^{\beta/2} d\bar{t} [\Sigma_c^{\lessgtr}(t_1, -i\bar{t})G^{\lessgtr}(-i\bar{t}, t_2) + \Sigma_c^{\lessgtr}(t_1, i\bar{t})G^{\lessgtr}(i\bar{t}, t_2)], & (29)
 \end{aligned}$$

with contributions also from the vertical track (the memory-effects, due to initial state correlations, during the time evolution); similar expressions read for the other time arguments and time derivatives (when one of two time arguments is complex, the collision integral I_1^{\lessgtr} also has contributions from Matsubara's propagators).

With $\mathfrak{h} = h + \Sigma_{\text{HF}}$, it is expedient to define [32] a single-particle operator S which satisfies $i\partial_{t_1} S(t_1, 0) = \mathfrak{h}(t_1)S(t_1, 0)$, with $S(0, 0) = S^\dagger(0, 0) = 1$ and $S(t_1, \bar{t})S(\bar{t}, t_2) = S(t_1, t_2)$. S is a matrix in the single-particle labels [32]. Using the unitary gauge transformation $G^{\lessgtr}(t_1, t_2) = S(t_1, 0)g^{\lessgtr}(t_1, t_2)S^\dagger(t_2, 0)$, after some algebra we arrive at the following expression for $G^>$ at time $T_p + \Delta$:

$$G^>(T_p + \Delta, t_2) = S(T_p + \Delta, T_p)G^>(T_p, t_2) - iS(T_p + \Delta, T_p) \int_0^\Delta S^\dagger(\bar{t} + T_p, T_p) T_1^>(\bar{t} + T_p, t_2). \quad (30)$$

Similar expressions hold for the other Green's functions. To perform the actual integration on the numerical time-grid, it is expedient to divide the time-step Δ in N sub-intervals, to obtain

$$S(T_p + \Delta, T_p) = \prod_{j=0}^{N-1} e^{-i\mathfrak{h}(t_j)\Delta_N} \quad (31)$$

where $\Delta_N = \Delta/N$, $t_j = T_p + (j + 1/2)\Delta_N$, and with $\mathfrak{h}(t)$ evaluated with a four-point extrapolation/interpolation. To solve (30) the integral is approximated numerically with a low-order discretization formula. The other KBE are computed similarly, but special care must be exerted for the diagonal contributions, when $t_1 = t_2$. We defer to the original literature for details [28–30, 32].

To summarize, solving the KBE (within a perturbative many-body scheme) in the time interval $[T_p, T_p + \Delta]$ is accomplished in two nested loops. The outer loop (which makes use of a predictor-corrector scheme) starts with an approximate propagation of (23) and (24) to get an approximate \tilde{G} . Then, via an inner loop, self-consistency (for, e.g., T , see (26)) is achieved, where the quantities depend on the input \tilde{G} . The iterative process ends when self-consistency is achieved, and the process restarts for the next time step.

5 Linear Response via the KBE

Is there any advantage in using the KBE for weak perturbations?

If the perturbation is weak and the linear order of the response to the perturbation is sufficient (an example of weak perturbation is the probe pulse in time resolved optical spectroscopy), the near equilibrium properties can be computed by linear response theory (Kubo [33, 34]). In Kubo's theory a response function satisfies the so-called Bethe–Salpeter equation (see below), which can be solved in the frequency domain. The solution is quite demanding to implement numerically and, in general, this has mostly been done for relatively simple kernels. It turns out that the KBE can also be used to perform linear response calculations, while avoiding the direct solution of the Bethe–Salpeter equation.

In the linear regime, we are interested in the response of the NEGF to the small variation of the perturbing potential $u(t, \mathbf{r})$:

$$\frac{\delta G(1, 2)}{\delta u(3)} \Big|_{u=0} = -L(1, 3, 3^+, 2) = -G_2(1, 3, 3^+, 2) + G(1, 2)G(3, 3^+) \quad (32)$$

where L is called the response function and is related to the two-particle Green's function G_2 , which has already appeared in (22). Sometimes it is convenient to generalize the equations to non-instantaneous (and non-local) external potentials $w(t, \mathbf{r}, t', \mathbf{r}')$

$$\frac{\delta G(1, 2)}{\delta w(4, 3)} \Big|_{w=0} = -L(1, 3, 4, 2) = -G_2(1, 3, 4, 2) + G(1, 2)G(3, 4), \quad (33)$$

to appreciate fully the structure of the time dependence. As mentioned before, the central quantity in the NEGF is the non-equilibrium Green's function $G(t_1, t_2)$, from which the addition/removal spectrum, the density, and the current can be extracted. On the other hand, the key aspect in linear response theory is the excitation spectrum, which can be extracted from the density–density response function, $\chi(1, 2) = \frac{\delta n(1)}{\delta u(2)} \Big|_{u=0} \approx \langle \hat{\psi}^\dagger \hat{\psi} \hat{\psi}^\dagger \hat{\psi} \rangle$ [35, 36]. The corresponding change in the density, $n(1)$ has the form

$$\frac{\delta n(1)}{\delta u(3)} \Big|_{u=0} = iL(1, 3, 3^+, 1^+). \quad (34)$$

To see the connection with the NEGF we use the construction of the density from the lesser Green's function $n(1) = -iG^<(1, 1) = -iG(1, 1^+)$. Then the analytic pieces of the response function are

$$\begin{aligned} \frac{\delta G^<(1,1)}{\delta u(3)} \Big|_{u=0, t_1 > ct_3} &= -L(1, 3, 3^+, 1^+)_{t_1 > ct_3} = -i\chi^>(1, 3) \\ \frac{\delta G^<(1,1)}{\delta u(3)} \Big|_{u=0, t_1 < ct_3} &= -L(1, 3, 3^+, 1^+)_{t_1 < ct_3} = -i\chi^<(1, 3) \end{aligned} \quad (35)$$

The retarded density–density function is defined as

$$\chi^R(1, 3) = \theta(t_1 - t_3)(\chi^>(1, 3) - \chi^<(1, 3)), \quad (36)$$

and can be computed making use of the Bethe–Salpeter equation

$$\begin{aligned} L(1, 3, 4, 2) &= L_0(1, 3, 4, 2) \\ &- \int_{\gamma} L_0(1, 5, 6, 2) \Gamma(6, 8, 7, 5) L(7, 3, 4, 8) d5d6d7d8. \end{aligned} \quad (37)$$

where $L_0(1, 3, 4, 2) = -G(1, 4)G(3, 2)$. The equation, to be solved, requires an approximation for the kernel Γ . However, even for rather simple kernels, this is a difficult task because of the four-point structure of the equation. One way to proceed is to devise kernels via the generating potential (see Fig. 2):

$$\frac{\delta\Phi}{\delta G(2, 1)} = \Sigma(1, 2), \quad (38)$$

$$\frac{\delta\Sigma(1, 2)}{\delta G(4, 3)} = \Gamma(1, 3, 4, 2), \quad (39)$$

and this ensures that the conservation laws [23, 25, 26] are obeyed.

On the other hand, one can extract the retarded density–density response function χ^R by inverting the integral

$$\delta(-iG^<(1, 1)) = \int_{t_0}^{\infty} \theta(t_1 - t_3)(\chi^>(1, 3) - \chi^<(1, 3))\delta u(3)d3, \quad (40)$$

if one knows $\delta G^<(1, 1)$. The change in $G^<$ can be conveniently computed with the NEGF. The equation is usually solved in the steady-state limit (where all quantities depend on the time difference) using the Fourier transform:

$$\delta n(\omega) = \chi^R(\omega)\delta u(\omega). \quad (41)$$

To mention an application, such a procedure was used [10] to characterize the dipole moment of a molecule under the influence of an external electric field. In terms of the response function transformed to the time domain, the dipole moment for a field E_0 in the direction z , reads (see [10] for further details)

$$d(t) = E_0 \int z' \chi^R(\mathbf{r}, \mathbf{r}', t) z d\mathbf{r} d\mathbf{r}'. \quad (42)$$

We conclude this section by noting that simple approximations for the KBE are translated to highly non-trivial kernels of the BSE, and time-propagation of the KBE offers a direct method to calculate response functions and excitation energies. This can be of great relevance for first-principles treatments. An implementation of the KBE at the ab initio level is discussed next.

6 A Recent Ab Initio Application of the KBE

We have seen that the full numerical solution of the time-dependent KBE requires the evaluation and integration of several different double-time quantities on the time square (t, t') . Computationally this can already be demanding for simple model systems (see, e.g., the discussion in [29, 30, 37]): Thus, an appropriate question is whether, for real materials, an ab initio solution of the KBE is possible at all.

If one is willing to specialize the treatment in some way, and to consider a number of approximations, an ab initio KBE approach becomes viable. This strategy, which paves the way to a systematic KBE treatment of materials (with

electronic and lattice structures fully taken into account), was recently introduced [38, 39] and applied to Si bulk; its main aspects are briefly reviewed here, following closely the presentation style and notation of the original works [38, 39].

To circumvent the issue of a computationally costly double-time structure, one can specialize the KBE to the $t = t'$ axis in terms of a time derivative with respect to both time arguments. Also, in an ab initio approach, it is convenient to express all quantities in a KS basis $\{\varphi_{m\mathbf{k}}(\mathbf{r})\}$. For example, in the KS basis, the Green's function is expressed as

$$G(1, 2) = \sum_{m', \mathbf{k}} \varphi_{m\mathbf{k}}^*(\mathbf{r}_1) G_{m'\mathbf{k}}(t_1, t_2) \varphi_{m'\mathbf{k}}(\mathbf{r}_2). \quad (43)$$

The KS basis is obtained by solving the KS equations

$$\left[-\frac{\nabla^2}{2} + V_{\text{KS}}(\mathbf{r}) \right] \varphi_{m\mathbf{k}}(\mathbf{r}) = \varepsilon_{m\mathbf{k}} \varphi_{m\mathbf{k}}(\mathbf{r}), \quad (44)$$

where V_{KS} describes the effect of the ionic potential and of the electron–electron interactions (schematically, $V_{\text{KS}} = V_{\text{ion}} + V_{\text{Hartree}} + V_{\text{xc}}$, where the electronic part is divided into a Hartree and an XC contribution). Within the KS basis, when the time-dependent perturbation \hat{U} maintains the spatial symmetry of the system (for example $\hat{U}(t) = -e\hat{\mathbf{r}} \cdot \mathbf{E}(t)$) and the momentum \mathbf{k} is conserved, the equation of motion for the equal-time lesser component of G becomes [38, 39]

$$i \frac{\partial}{\partial t} \mathbf{G}_{\mathbf{k}}^<(t, t) = [\mathbf{h}_{\mathbf{k}}^{\text{KS}} + \mathbf{V}_k^{\text{Hartree}}(t) + \Sigma_{\mathbf{k}}^s(t) + \mathbf{U}_k(t), \mathbf{G}_{\mathbf{k}}^<(t, t)] + \mathbf{S}_{\mathbf{k}}^<(t). \quad (45)$$

In (45), all quantities should be understood as matrices in the index m, m' , e.g., $(\mathbf{G}^<)_{mm'} \equiv G_{mm'}^<$. Furthermore, the structure of the RHS of (45) is a commutator $[\dots, \mathbf{G}^<]$ plus an inhomogeneous term $\mathbf{S}_{\mathbf{k}}^<(t)$. The commutator originates from performing the time derivative with respect to both time arguments of $(\mathbf{G}^<)_{mm'}$ (cf. with the one-sided time derivative of $G^<$; see (28) and (29)).

Besides $\mathbf{G}^<$, the other terms in the commutator are the KS equilibrium Hamiltonian $\mathbf{h}_{\mathbf{k}}^{\text{KS}}$, the time-dependent Hartree term $\mathbf{V}_k^{\text{Hartree}}$, the external field \mathbf{U}_k , and a self-energy contribution $\Sigma_{\mathbf{k}}^s$, introduced to take into account static correlations, so that in the linear regime one recovers the Bethe–Salpeter equation from the KBE [38, 39]. The remaining term in the RHS, $\mathbf{S}_{\mathbf{k}}^<(t)$, is the one containing the dynamical scattering effects due to interactions among electrons or between electrons and phonons. Its explicit form reads [39]

$$\mathbf{S}_{\mathbf{k}}^<(t) = \int_{-\infty}^t d\bar{t} [\Sigma_{\mathbf{k}}^>(t, \bar{t}) \mathbf{G}_{\mathbf{k}}^<(\bar{t}, t) + \mathbf{G}_{\mathbf{k}}^<(t, \bar{t}) \Sigma_{\mathbf{k}}^>(\bar{t}, t)] - (\lesseqgtr \rightarrow \gtrless), \quad (46)$$

where the second contribution on the RHS is obtained by interchanging lesser with greater functions in the integral. The expression for $\mathbf{S}^<$ is again the result of

performing a time derivative in both arguments (thus producing the sum of two mutually adjoint contributions), and of applying Langreth's rules [31] to translate quantities from the Keldysh-contour to the physical time-axis. We wish to add that in the original treatment of [39], electron-phonon interactions are explicitly included, with the phonons assumed to be in thermal equilibrium at a phonon bath temperature β^{-1} . Thus there is a dependence on β in the quantities of (45) and (46) which, however, for the scopes of our cursory overview does not need to be further considered. In Marini [39], additional simplifications are introduced to perform the actual simulations. First, the electronic contribution to the self-energy is calculated within the GW approximation (see, e.g., [40]), with the screened interaction W calculated at the static level. Second, the boson-propagators which enter the phononic part to Σ are determined using the equilibrium phonon distributions. Third, $G_{mm'\mathbf{k}}$ and $\Sigma_{mm'\mathbf{k}}$ are taken as diagonal in the m indexes (for example, $G_{mm'\mathbf{k}}(t, t) \approx i\delta_{mm'}f_{m\mathbf{k}}(t)$, where $f_{m\mathbf{k}}$ are the electronic occupations). Even with all these approximations considered, a further simplification is required since, in (45) and (46), $\mathbf{S}^<$ contains double-time quantities and thus the equation for $\mathbf{G}_{\mathbf{k}}^<(t, t)$ is still not closed. The latter difficulty can be circumvented by introducing the so-called *Generalized Kadanoff-Baym Ansatz* (GKBA) [41, 42], which is an approximate decoupling procedure:

$$G_{m\mathbf{k}}^<(t, t') \approx i[G_{m\mathbf{k}}^R(t-t')G_{m\mathbf{k}}^<(t', t') - G_{m\mathbf{k}}^<(t, t)G_{m\mathbf{k}}^A(t-t')]. \quad (47)$$

In Marini [39], it is shown how to compute $\mathbf{S}^<$ in terms of $G^{R,A}$ and the electronic occupations $f_{m\mathbf{k}}$. The final expression for $\mathbf{S}^<$ (and the relative algebraic derivation) is rather cumbersome, but the $G^{R,A}$ are assumed to have exponential behavior (i.e., the transient, non-exponential features are neglected), and this additional assumption permits the analytical evaluation of the time-integrals. Eventually, one ends up with a set of (particle-number conserving) coupled nonlinear differential equations for the time evolving electronic occupations $f_{m\mathbf{k}}(t)$:

$$\frac{\partial f_{m\mathbf{k}}(t)}{\partial t} = \left[\frac{\partial f_{m\mathbf{k}}(t)}{\partial t} \right]_{\text{coh.}} - S_{m\mathbf{k}}^<(t), \quad (48)$$

$$\left[\frac{\partial f_{m\mathbf{k}}(t)}{\partial t} \right]_{\text{coh.}} = -[\mathbf{h}_{\mathbf{k}}^{\text{KS}} + \mathbf{V}_k^{\text{Hartree}}(t) + \Sigma_{\mathbf{k}}^s(t) + \mathbf{U}_k(t), \mathbf{G}_{\mathbf{k}}^<(t, t)]_{mm} \quad (49)$$

where $S^<$ is expressed in terms of the electronic occupations $\{f_{m\mathbf{k}}(t)\}$ and of the lifetimes due to repeated electron-electron and electron-phonon scattering processes. Thus the de-excitation and decay of electrons occur via the possible creation of electron-hole pairs and phonons. In Marini [39], a discussion of the non-equilibrium behavior of Si bulk is provided starting from a specific excited electronic initial state, and a clear illustration of de-excitation via different channels is provided, with the main conclusion that, due to the electronic gap and for near-threshold excitations, decay via the electron-phonon channels dominates over the electron-electron one in the short-time dynamics.

We refer the interested reader to the original papers [38, 39] for detailed results for silicon. As an outlook to this section, the approach of [39] represents a significant methodological advance in the *ab initio* treatment of the time-dynamics of solids and time-resolved spectroscopies. At the same time, the different approximations/assumptions introduced to make it computationally viable certainly require further scrutiny and validation. In line with the aims of this chapter, an main issue is then how to deal with electron–electron interactions in the case of strongly correlated materials out of equilibrium (e.g., if/when to improve over the GW scheme). This is discussed in what follows.

7 Learning from Models

Can the study of model systems shed light on how to describe strongly correlated systems out of equilibrium (and thus time-dependent spectroscopies)?

For many materials, the GW approximation provides an accurate many-body description of the electronic structure (see the chapter by Bruneval and Gatti in this book). On the other hand, in the case of strongly correlated systems, successful options exist based on non-perturbative methods (chapter by Biermann). However, even in the static case, the implementation of non-perturbative schemes at the *ab initio* level is computationally intensive, and for materials with cells of moderate size. In view of this, their use for an *ab initio* description of the non-equilibrium regime appears to be impracticable at present, due to the double-time structure of the NEGF. As we have just seen, even in the “simple” case of Si, one has to resort to a series of approximations, and simplified GW self-energies, to make the *ab initio* NEGF scheme tractable. Thus we can ask: what is the scope of approximations such as GW, 2nd Born, or *T*-matrix for strongly correlated systems? Considerable insight can be obtained by studying simple model systems, and here we focus on lattice Hamiltonians. The model we use in our discussion is the time-dependent inhomogeneous Hubbard Hamiltonian, which in standard notation reads

$$H = \sum_{i\sigma} \varepsilon_i \hat{n}_{i\sigma} - V \sum_{\langle ij \rangle, \sigma} a_{i\sigma}^\dagger a_{j\sigma} + \sum_i U \hat{n}_{i\uparrow} \hat{n}_{i\downarrow} + \sum_{i\sigma} w_i(t) \hat{n}_{i\sigma}. \quad (50)$$

Compared to the standard Hubbard Hamiltonian [43], in (50) there is an extra, time-dependent term representing the dynamical perturbation. In what follows, $V = 1$, i.e., it is taken as an energy unit. We now use this model to compare many-body approximate treatments to exact ones for finite clusters. Before considering the dynamics, we start by looking at equilibrium spectral functions, since in this case we can also extract some interesting features [28]. Figure 4 shows results for fairly strong interactions ($U = 4$) in the case of a six-site chain. Away from half-filling is a regime where the TMA is expected to work well, and in fact we see that the TMA provides a fairly good description of the spectral function, including the

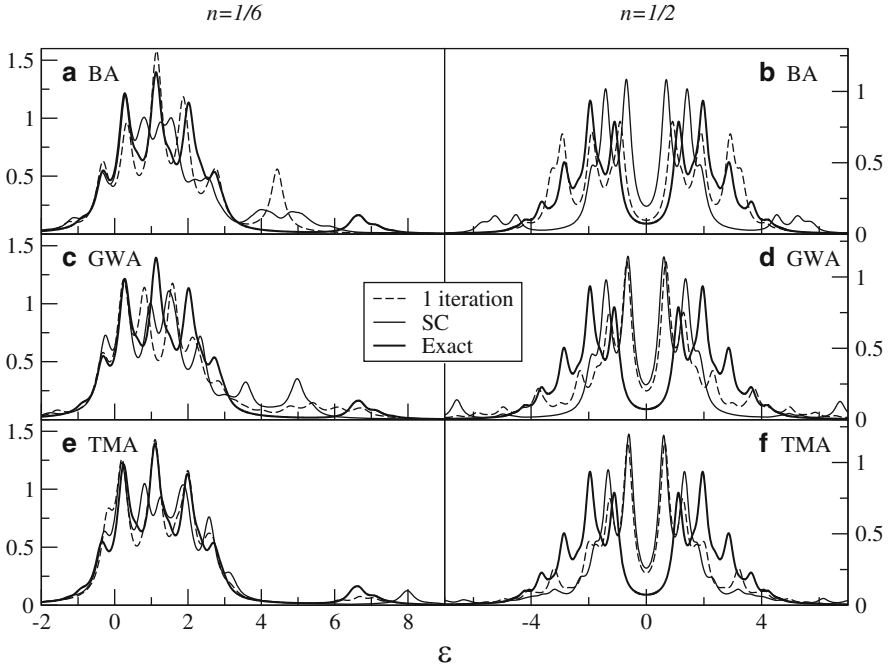


Fig. 4 Exact vs approximate results for the spectral function of six-site, open ended Hubbard chains with $U = 4$. The approximations used are 2nd Born (BA), the GW approximation (GWA), and the T -matrix approximation (TMA). Two different densities are considered, $n = 1/6$ and 0.5 , and for the approximate treatments, both one-only iteration and full self-consistent results are shown (adapted from [28, 30])

split-off structure at energy $\varepsilon \approx 6$, also consistent with other comparative studies [44–46]. On the other hand, BA and GWA are definitely inferior to TMA, and completely unable to account for the satellite region. At half-filling, the performance of the different MBA worsens, and now it is the BA to provide the closest (and yet, very little) agreement with the exact result (for example, the gap value is best represented in the BA). As a general feature in Fig. 4, the self-consistent solution for the spectral function does not improve over the one-shot case and, in some cases, see, e.g., Fig. 4e, rather the opposite occurs. This is not unexpected, since self-consistency in partial diagrammatic summations is a requirement to get conserving approximations, but can in fact worsen spectral densities [5, 44, 47].² The non-equilibrium behavior of the system is shown in Fig. 5. The results were obtained by numerically solving the KBE as described earlier and the time-dependent perturbation used is a sudden shift of the on-site energy of the first site of the chain. Looking at Fig. 5, the agreement between MBA and exact results is

² Naturally, the agreement between MBA and exact solutions improves by reducing the value of U , but at the same time the results become increasingly close to the non-interacting ones.

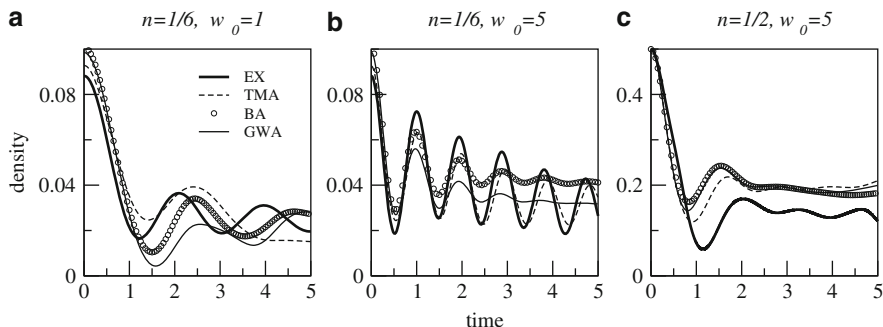


Fig. 5 Exact vs approximate results for the time-dependent density at the first site of a six-site Hubbard chain after the sudden switch-on of a perturbation at the same site. The approximations used are the BA, GWA, and TMA. Two different cluster fillings and two values of the perturbation strength w_0 are considered (adapted from [28, 30])

comparable (or inferior) to the static case. Also, at low filling, the TMA performs better than the other MBA irrespective of the perturbation strength w_0 . However, TMA and exact curves are mutually closer at larger w_0 values (for small w_0 , the dynamics primarily involves the band region of the spectrum, which is not well reproduced by the TMA). One-dimensional systems are certainly quite a severe test for the different MBA we considered, so one can wonder whether the MBA performance would improve, say, for example, in 3D. Related to this, there is a second relevant question: in which way should one improve over the MBA? In the KBE formulation just discussed, the self-energies are matrices in the site-indexes, i.e., no local approximations (such as, e.g., in single-site Dynamical Mean Field Theory, DMFT) are made. Furthermore, when solved in time (i.e., not at the steady state) the KBE fully take into account memory effects (i.e., the history of the system). Thus, improving the MBA must necessarily introduce a better treatment of electron-correlations. We will come back to this point later on. For the moment, we make a digression and introduce another approach to the real-time dynamics of the Hubbard model, namely time-dependent density functional theory in its lattice version.

8 DFT and TDDFT (in the Lattice Version)

To gain insight on how to treat electronic correlations in time-dependent spectroscopies, we find it useful to look at density-functional theory methods.

Static [48, 49] and time-dependent [50] density-functional theory (DFT and TDDFT, respectively) have been discussed in detail in several other chapters of this book (for TDDFT, see in particular the contribution by Sharma et al.). The importance of (TD)DFT for an ab initio description of real materials cannot be overemphasized: nowadays DFT is the premier tool for the investigation of the

static properties of many materials, whilst TDDFT is playing an increasingly important role for describing electronic excitations. The practical implementation of (TD)DFT resorts to a fictitious non-interacting system, the Kohn–Sham (KS) system [48–51]. Central to the KS scheme is v_{xc} , the XC potential, which accounts for all the many-body effects. If no approximations are made for v_{xc} , the one-particle density of the many-body system is exactly obtained in terms of the single-particle states of the KS system. However, in general the exact v_{xc} is not known (it is a highly non-trivial functional of the density, and in TDDFT it also depends on the initial state), and different approximate choices are possible. Relevant to the rest of this chapter, we mention two very simple ones: the local density approximation (LDA) for DFT (where v_{xc} depends only on the local density) and the adiabatic LDA (ALDA) for TDDFT (where v_{xc} has an instantaneous dependence on the local density). For a more detailed discussion of DFT and TDDFT, we refer the reader to excellent and comprehensive reviews and books [52–55]. For the lattice versions of DFT (LDFT) [56–58] and TDDFT (LTDDFT) [59–63], the site occupation number is the basic variable. Recent reviews of L(TD)DFT can be found in [64, 65]. For the present scopes, we limit our discussion to the (inhomogeneous) 3D Hubbard model within the (A)LDA. As in the continuum case, the functional dependence of v_{xc} on the density is obtained from the ground-state energy of the appropriate homogeneous reference system, in this case the 3D infinite and homogeneous Hubbard model.

In Karlsson et al. [66], the ground state energy was calculated within DMFT [67–69] in the single-site approximation. Single-site DMFT is non-perturbative and variational in character, and generally gives reliable ground-state energies. In fact, single-site DMFT is also often accurate in two-dimensions (see, e.g., the comparisons to Dynamical Cluster Approximation and diagrammatic Quantum Monte Carlo [70]; for a comprehensive discussion of DMFT, see the chapter by Biermann). From DMFT, the functional form of $v_{xc}^{\text{hom}}(n)$ is obtained as [66]:

$$v_{xc}^{\text{hom}}(n) = \frac{\partial}{\partial n} (E_{\text{DMFT}}[n] - T_0[n] - Un^2/4), \quad (51)$$

where $T_0[n]$ and $Un^2/4$ are the kinetic-energy density of the non-interacting system and the Hartree energy density, respectively. The XC potential from (51) is shown in the left part of Fig. 6: it is easily noted that a discontinuity at half-filling emerges when the strength of the Hubbard interaction U is above a critical value U_{crit} . This is how the Mott–Hubbard metal-insulator transition (signaled, e.g., by an infinite mass renormalization or by a vanishing Drude’s weight) manifests within LDFT for a 3D system. In lower dimensions, the situation can be different: we are not aware of studies of v_{xc} for the 2D Hubbard model, but in 1D there are several papers dealing with LDFT [64]; in this case the metallic phase occurs only at $U = 0$, i.e., for any $U > 0$ a gap is present (such a gap becomes exponentially small for $U \rightarrow 0$), the system is always in the Mott phase, and there is always a discontinuity in v_{xc} . In 3D, at half-filling, the discontinuity in v_{xc} only shows up for all $U > U_{\text{crit}}$ (the size of the discontinuity increases for increasing U values). As shown in the right side of Fig. 6,

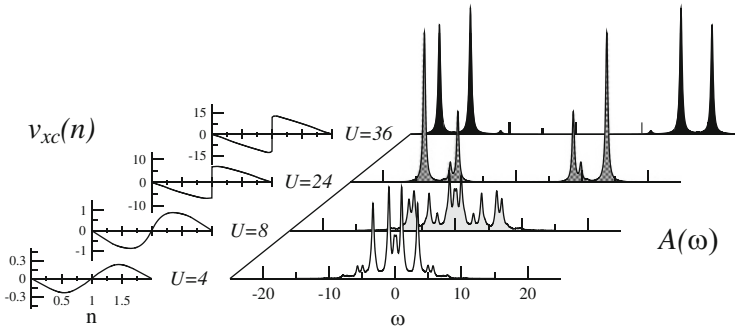


Fig. 6 The XC potential for the 3D homogeneous Hubbard model as obtained from Dynamical Mean Field Theory. Results for v_{xc} as a function of the density and for the many-body spectral function $A(\omega)$ are shown for several values of the interaction U

results for the DMFT spectral function $A(\omega)$ also support this picture: we observe a gapped spectrum only at finite U values, with the gap size increasing at large interaction strengths. Finally, we note that a similar behavior is arrived at if one consider the Gutzwiller approximation (GA) or Quantum Monte Carlo results (for example, DMFT and GA give close values for U_{crit} ; see the chapter by Biermann).

In terms of v_{xc} from (51), it is now possible to introduce an (A)LDA for the inhomogeneous case. Preliminary to a TDDFT calculation, the ground state of an inhomogeneous Hubbard system is obtained via the self-consistent KS equations:

$$(\hat{T} + \hat{v}_{\text{KS}})\psi_k = \epsilon_k \psi_k, \quad (52)$$

where, in the lattice-site picture, the KS potential $v_{\text{KS}}(i) = v_{\text{ext}}(i) + Un(i)/2 + v_{xc}(i)$, and \hat{T} is the lattice kinetic energy operator. In v_{KS} , the three terms denote the external potential, Hartree, and XC contributions, respectively. In the LDA, $v_{xc}(i) \approx v_{xc}^{\text{hom}}(n(i))$, with $n(i) = 2 \sum_{k \in \text{occ}} |\psi_k(i)|^2$. Here, the factor 2 comes from spin degeneracy, and the k -sum involves the occupied KS orbitals.

For the TDDFT real-time dynamics, the time-dependent KS equations read

$$(\hat{T} + \hat{v}_{\text{KS}}(t))\psi_k(t) = i\partial_t \psi_k(t), \quad (53)$$

where $v_{\text{KS}}(i, t) = v_{\text{ext}}(i, t) + Un(i, t)/2 + v_{xc}(i, t)$, $n(i, t) = 2 \sum_{k \in \text{occ}} |\psi_k(i, t)|^2$ and, in the ALDA, $v_{xc}(i, t) = v_{xc}^{\text{hom}}(n(i, t))$.

We conclude this digression about L(TD)DFT by mentioning that it can also be used in the linear response regime [71] (for a discussion of linear response TDDFT in the continuum case, see the chapter by Sharma et al.). For the lattice case, the XC kernel f_{xc} is defined as (n_{gs} is the ground state density)

$$f_{xc}(\mathbf{R}, \mathbf{R}'; t, t') = \left. \frac{\delta v_{xc}(\mathbf{R}, t)}{\delta n_{\mathbf{R}'}(t')} \right|_{n=n_{\text{gs}}}. \quad (54)$$

In the ALDA, $f_{xc}^{\text{ALDA}}(\mathbf{R}, \mathbf{R}'; t, t') = v'_{xc}(n_{\text{gs}})\delta_{\mathbf{R}-\mathbf{R}'}\delta(t-t')$, i.e, the dependence on space and time variables becomes local. Thus, for the homogeneous 3D Hubbard model, $f_{xc}^{\text{ALDA}}(\mathbf{q}, \omega) \equiv f_{xc}$, which depends only on the uniform ground-state density n_{gs} . Then the response function in the ALDA is (U is the Hubbard interaction strength)

$$\chi(\mathbf{q}, \omega) = \frac{\chi_0(\mathbf{q}, \omega)}{1 - (U + f_{xc})\chi_0(\mathbf{q}, \omega)}, \quad (55)$$

where, in analogy with the continuum case, $\chi_0(\mathbf{q}, \omega)$ is the response of the KS system.³

In Verdozzi et al. [71], f_{xc} in the DMFT-ALDA was used to compute the response function of the 3D homogeneous Hubbard model, and, from it, the local double-occupancy $d_{\mathbf{R}} = \langle \hat{n}_{\mathbf{R}\uparrow}\hat{n}_{\mathbf{R}\downarrow} \rangle$. The results showed that the ALDA double occupancies can become slightly negative (a well-known feature exhibited by the RPA in the continuum case), but that problem might be less severe than in the continuum case, due to the discrete nature of the lattice.

9 Strongly Correlated Materials Out of Equilibrium: KBE or TDDFT?

The KBE and TDDFT are in principle exact treatments of the non-equilibrium problem. Furthermore, a formal link can be established between TDDFT and MBPT via the so-called Sham–Schlüter equation, which relates the XC potential to the electron self-energy [72, 73]:

$$\int_{\gamma} d2G_{\text{KS}}(1, 2)[v_{\text{KS}}(2) - v_{\text{ext}}(2)]G(2, 1) = \int_{\gamma} d2d3G_{\text{KS}}(1, 2)\Sigma(2, 3)G(3, 1), \quad (56)$$

which is obtained by using the Dyson equation and considering that for both the many-body system and the KS systems (G_{KS} denotes the KS propagator) the electron density is $n(1) = -iG(1, 1^+) = -iG_{\text{KS}}(1, 1^+)$. Naturally, a difference between results from the NEGF and TDDFT approaches can be made by the level of approximations one introduces in v_{xc} and/or Σ in actual implementations, and this is what motivates our question in the title of this section.

³Equations (54) and (55) are written for a spin-independent treatment, to stress the analogy with the continuum case. However, the Hubbard interaction, (50), is written in spin-dependent form, i.e., exchange is already removed at the Hamiltonian level. Thus, to be consistent, in (55) one should perform the replacement $f_{xc} \rightarrow f_{xc} - U/2$; see [71] for more details.

We now make a comparative assessment of the different approximations schemes for the KBE and TDDFT discussed in Sects. 4, 7, and 8. This comparison was originally considered in [66, 71], using a simple 3D model system which can be solved exactly and in terms of MBA and ALDA-DMFT.⁴ The system is a cubic cluster with 5^3 sites, described by a single-orbital tight-binding, nearest-neighbor hopping Hamiltonian, with a Hubbard-type interaction $U\hat{n}_{0\uparrow}\hat{n}_{0\downarrow}$ at the central site. With the use of symmetry, the cluster can be numerically solved exactly for the densities at the central site, provided that the time-dependent perturbation is also confined at that site.

Results for slow and sudden perturbation were both considered in [66, 71] to contrast the different aspects due to electron correlations. The results from such calculation are displayed in Fig. 7a–e, while in Fig. 7f we show the ten-site symmetry-adapted system and the (Gaussian) shape of the slow perturbation at the interacting, central site (the sudden perturbation is proportional to the step function $\theta(t)$). In Fig. 7, the particle density (the number of particles in the initial, ground state), the strength of the interactions, and the “speed” and strength of the time-dependent perturbation can be (and are) varied independently. This permits one to extract some interesting features of the interplay between correlations and memory effects due to interactions.

Starting with Fig. 7a, we see that for moderate interactions (in this model, and in units of the hopping parameter, $U = 8$ and the “bandwidth” $W \lesssim 12$), there is excellent agreement in time between all the MBA and the ALDA-DMFT with the exact solution. This is because, for the slow perturbation in Fig. 7a, neither strong correlation effects (which require to go beyond the MBA that we used), nor non-adiabatic effects (beyond ALDA) appear to be very important. The situation changes in Fig. 7b: this is a clear case of strong correlation regime ($U = 24$), but the perturbation remains slow; the MBA become clearly inadequate, but ALDA-DMFT still gives a good description: the inclusion of non-perturbative effects (as in ALDA-DMFT) appears to be relatively more relevant than taking into account memory effects. Yet other changes are observed in Fig. 7c–e, where a sudden perturbation and only moderate interactions $U = 8$ are considered. In this case, non-adiabaticity becomes highly relevant and a dependence on the perturbation strength is also apparent. In Fig. 7c, results for the low-density limit are shown. This is when the TMA (but not the BA or the GWA) is expected to perform well, and in fact exact and TMA results are virtually indistinguishable. Since the perturbation strength is small (0.2), even ALDA-DMFT performs well initially, but rapidly deteriorates due to the lack of memory effects. In Fig. 7d, the increase of the perturbation strength induces a clear failure of ALDA-DMFT (suggesting that including memory effects is even more necessary), while also considerably worsening the quality of the TMA results (the strong attractive perturbation suddenly

⁴ A comparison of this kind has also been made in 1D for a quantum transport geometry [74] in terms of KBE, time dependent density-matrix renormalization group results, and LTDDFT within an ALDA for the inhomogeneous 1D Hubbard model [59].

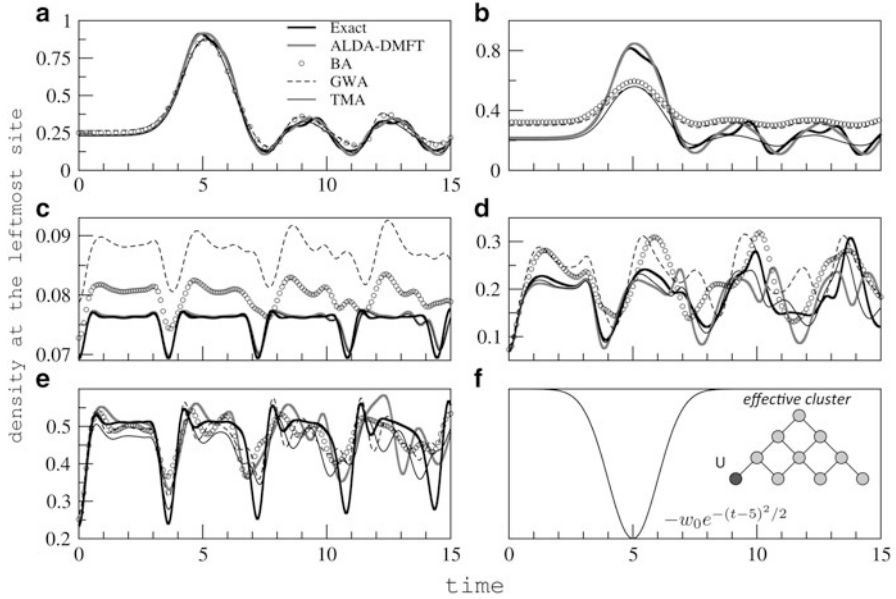


Fig. 7 Exact, KBE, and TDDFT-DMFT dynamics for a $5 \times 5 \times 5$ cluster, with a central interacting site. The external field $w(t)$ is applied at the impurity site. Using O_h symmetry, the time-dependent density of this site can be exactly reproduced within a ten-site effective cluster (**f**, dark circle). The specification for the curves in (**a**–**e**) is given in (**a**). For (**a**, **b**), a Gaussian perturbation $w(t) = -w_0 \exp[-0.5(t - 5)^2]$ is considered (see **f**), while a step perturbation $w(t) = -w_0 \theta(t)$ is used in (**c**–**e**). In (**c**–**e**) the value of the densities for $t \leq 0$ is the unperturbed, ground state one (such value is shown for $t = 0$). The specific parameters are: (**a**) $U = 8, N = 4, w_0 = 5$; (**b**) $U = 24, N = 4, w_0 = 5$; (**c**) $U = 8, N = 2, w_0 = 0.2$; (**d**) $U = 8, N = 2, w_0 = 2$; (**e**) $U = 8, N = 4, w_0 = 2$ (adapted from [71])

increases the density at interacting site beyond the range where the TMA performs well); the picture is the same at higher densities (Fig. 7e). Results for higher U , not shown, show an even poorer agreement between exact and approximate solutions. Finally, it is perhaps worth noting that BA and GWA are rather inadequate for most cases considered.

Extrapolating the above findings to the general case, we surmise that the description of strongly correlated materials out of equilibrium requires non-perturbative treatments of the interactions and a proper account of memory effects.⁵

⁵ Memory effects can be important even for a non-interacting system, since memory emerges from an embedding procedure for part of the system's degrees of freedom. When electronic correlations are important, memory effects can be harder to account for properly (because strong correlations are more difficult to account for properly). As a matter of fact, electronic correlations can even wash out memory, but in general this cancellation effect is quite difficult to describe correctly.

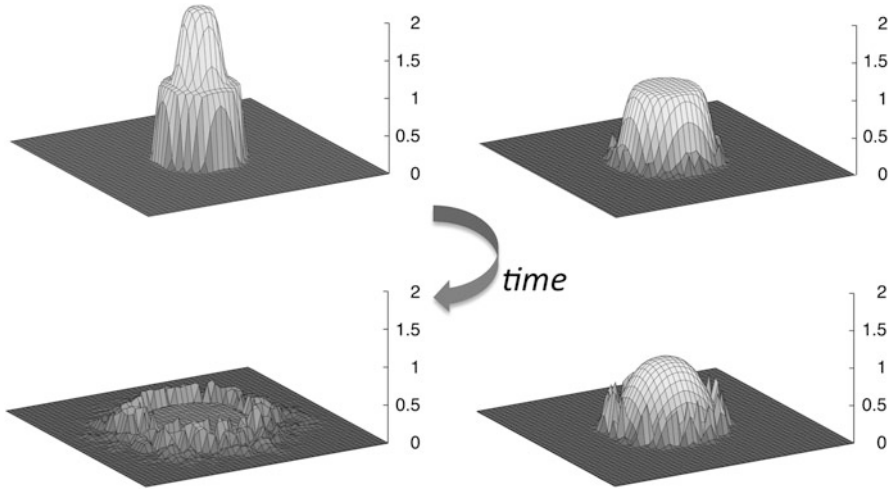


Fig. 8 Time-snapshots of a 3D interacting fermion cloud expanding in a disordered optical lattice. The cloud is initially ($t = 0$) confined by a harmonic potential. Results are obtained with lattice (TD)DFT-DMFT [66]. The time-ordering of the snapshots sequence is indicated by the curly arrow. The surface plots show the particle density in the $z = 0$ plane of a simple cubic cluster with 47^3 lattice sites. The system is described by a Hubbard model with substitutional disorder, and disorder is confined to a region surrounding the cloud in the initial state (*top left*). This system is of relevance to the study of ultracold fermions in optical lattices. Each site can accommodate at most two electrons with opposite spin, and the electronic cloud is made of $N \lesssim 1,000$ electrons in each spin channel. The density profile at $t = 0$ is the result of the competition between the confining potential and the Hubbard interaction ($U = 24$), and the flat density region at $n = 1$ (Mott-plateau) is a consequence of the discontinuity in v_{xc} , as computed with DMFT (adapted from [78])

In the past few years, non-perturbative NEGF schemes have appeared [75] for lattice models, which require dynamical auxiliary impurity solvers (see, e.g., [76, 77]) to attain the solution of the original lattice problem. While still in an early developmental phase in many respects, this avenue looks highly promising. However, NEGF propagation scales quadratically with the simulation time, and treatments at the *ab initio* level can be quite challenging. To clearly show the emergence of this hurdle, we show in Fig. 8 the dynamics of an assembly of fermions, performed within ALDA-DMFT [78]. The results concern the dynamical competition between lattice disorder and interactions for ultracold fermion atoms in optical lattices.⁶ To obtain meaningful results for inhomogeneous cases of Fig. 8 [78], the system studied must be taken large enough (in this case, the cluster has more than 10^5 lattice sites). Unless introducing substantial simplifications/approximations, this system size does not appear easily accessible to non-perturbative (indeed, even to perturbative), double-time NEGF schemes, even if one is dealing

⁶ Model Hamiltonians can give an accurate description in this case. Since many of the physical parameters of ultracold atoms in optical lattices can be experimentally tuned in independent ways and in a broad range, several theoretical issues in condensed matter can be unambiguously addressed.

with simple lattice Hamiltonians.⁷ At the same time, TDDFT appears to be able to cope with large inhomogeneous (model) systems, but there are no simple and practical ways to go beyond the ALDA (for the situation in the linear response regime, see the discussion in [53]).

Undoubtedly, there are many interesting cases which are not as extreme as those in Fig. 8; however, it is fair to say that our limited analysis of model systems suggests that, in general, substantial developments in both NEGF and TDDFT are needed to describe successfully the real-time dynamics of complex materials with strong correlations.

10 Conclusion and Outlook

In this chapter we have discussed some theoretical concepts of (ultrafast) time resolved spectroscopy applied to materials. It can be easily argued that the role of this technique is rapidly growing in importance among the experimental tools for materials-characterization. It is also fair to say that time-resolved materials characterization is in a rather early but fast developing stage. Thus, instead of attempting a comprehensive review of the current status of the field, and revisiting in a systematic way the connection between theory and experiment, we chose to consider a single (in our view) pivotal aspect, i.e., how theoretical approaches can/should deal with time-resolved spectroscopies for strongly correlated materials. A firm conceptual grip on this aspect is certainly an important necessary ingredient in the theoretical description (as a more utilitarian motivation for our strategy, this topic closely reflects our specific interests and research in the field). We have, furthermore, restricted ourselves to the NEGF technique and, to a lesser extent, to TDDFT, and we have used simple model systems to illustrate how the present state of development of these approaches deals with strongly correlated systems out of equilibrium. The overall outcome of our discussion is that substantial development is still needed for the XC potentials of TDDFT and the self-energies of the NEGF to be able to deal with strong correlation effects in complex materials out of equilibrium, especially for *ab initio* treatments.

Of course, ours is a largely extrapolated perspective, developed by looking at simple model systems; it is then legitimate to ask how much of what we said is of real consequence for the *ab initio* case. It is not easy to provide a general answer to this question, but we can try to add some brief considerations on a few recent theoretical developments that in our view are relevant for future advances in *ab initio* NEGF and TDDFT (and thus in theoretical time-dependent spectroscopy).

Starting with (TD)DFT, very recently the exact strong-interaction limit of the Hohenberg–Kohn energy density functional has been used as starting point to

⁷It may be useful to recall here that, with NEGF, several interesting quantities can be conveniently obtained, such equilibrium and non-equilibrium spectral functions, double occupancies [79], etc.

approximate the XC part of the KS approach [80] in the case of continuum systems. Desirable and crucial features such as a derivative discontinuity of the XC functional are well within the scope of the theory [81], and comparisons with benchmarks ground state results for 1D continuum systems are very encouraging [82]. Most likely this also means that an ALDA for continuum systems similar to the one discussed here for the 3D Hubbard model is certainly viable and one could reasonably expect a similar level of (good) agreement. However, in Sect. 9 we also concluded that it is very necessary to go beyond the ALDA (a similar outcome resulted from a recent study [83], where a non-adiabatic XC potential for a Hubbard dimer was proposed). In our view, the development of non-adiabatic potentials is the area where, at the moment, progress in general remains more uncertain.

For example, memory effects could be included via a variational approach to many-body theory, with the variational freedom of the functionals limited to non-interacting propagators determined by a local one-electron potential [73]. The quality of the XC potentials would then depend on the MBA for the action functional. However, recent exact results for the time-dependent XC potentials in few-electron continuum systems [84] show the emergence of dynamical step-like structures with non-local (in space and time) dependence on the density.⁸ Furthermore, a very recent treatment of photoemission within current density functional theory suggests the need of dealing with highly non-local correlations which connect sample and detector fields [85]. The kind of features we just mentioned can represent a serious hurdle in developing reliable approximations for v_{xc} . Finally, we also mention that, for the case of linear response, there are ongoing attempts to merge DMFT and TDDFT to obtain model non-local XC kernels (possibly to be generalized for ab initio treatments) [86].

For the NEGF, good progress has recently been made with the introduction of an ab initio scheme for the time-propagation on the time-diagonal axis [38, 39]. The method, reviewed in Sect. 6, uses a self-energy in the GWA for the interactions among electrons. In principle, other self-energies could be considered. In fact, our KBE benchmarks for Hubbard clusters suggest that, most likely, self-energies based on a number of well-known MBA (including the GWA used in [39]) might not be good enough for strongly correlated materials. In the latter case there exists a very promising line of attack based on non-perturbative, non-equilibrium methods that, to our knowledge, at the time of writing, are being considered for lattice models Hamiltonians (see, e.g., [75–77]). In our opinion, pursuing this avenue for real materials requires one to devise breakthrough strategies to reduce substantially the huge computational effort associated with an ab initio implementation. In this respect, a possibility could be represented by use of suitable extensions of the generalized Kadanoff–Baym ansatz [41] (already used in [39]) to devise accurate decoupling schemes for the time-integrals appearing in the KBE. Different research

⁸ We mention in passing that “unexpected” features in the exact XC potentials have also been observed in 1D Hubbard chains [59]; however, for LTDDFT, a proper interpretation also requires possible v -representability issues to be taken into account; see, e.g., [59, 61–63].

groups [87, 88] are currently working to broaden the scope and range of validity of this ansatz, with the long-term aim of rendering numerically viable *ab initio* NEGF schemes for inhomogeneous, strongly correlated materials. Another option (at least for model Hamiltonians) could be represented by strong-coupling approaches for the non-equilibrium regime, and dealing with large inhomogeneous systems via massively parallel computer architectures [89]. As a further possibility, one cannot exclude the possibility that progress could also come from hybrid approaches that merge at some level elements of TDDFT and NEGF. However, this issue remains beyond the scopes of this brief survey.⁹

In conclusion, the NEGF-KBE and TDDFT are two robust and comprehensive theoretical frameworks to describe time-resolved spectroscopy. Due to the availability of such powerful conceptual tools for the analysis of experiments, the future of this characterization technique looks unquestionably bright. At the same time, the limitations encountered by *ab initio* NEGF-KBE and TDDFT in their present states of development make it very clear that, in the coming years, a lot of effort needs to be put in by theoreticians to describe successfully the time-dependent spectral response of strongly correlated, inhomogeneous materials.

Acknowledgements Daniel Karlsson is gratefully acknowledged for critically reading the manuscript. Claudio Verdozzi wishes to thank Carl-Olof Almladh, Ulf von Barth, Daniel Karlsson, Alexey Kartsev, Antonio Privitera, and Marc Puig von Friesen for fruitful collaborations over the recent years on the topics of this chapter.

References

1. Eckstein M, Kollar M (2008) Theory of time-resolved optical spectroscopy on correlated electron systems. *Phys Rev B* 78:205119
2. Eckstein M, Kollar M (2008) Measuring correlated electron dynamics with time-resolved photoemission spectroscopy. *Phys Rev B* 78:245113
3. Eckstein M (2009) Nonequilibrium dynamical mean-field theory. PhD thesis, University of Augsburg, http://www.physik.uni-augsburg.de/theo3/Theses/eckstein_diss.pdf
4. Almladh C-O (1986) Importance of vertex corrections for obtaining correct selection rules in the theory of photoemission. *Phys Rev B* 34:3798–3806
5. Almladh C-O (2006) Photoemission beyond the sudden approximation. *J Phys Conf Ser* 35:127–144
6. Gumhalter B (2012) Stages of hot electron dynamics in multiexcitation processes at surfaces: general properties and benchmark examples. *Prog Surf Sci* 87(5–8):163–188
7. Krausz F, Ivanov M (2009) Attosecond physics. *Rev Mod Phys* 81:163–234
8. Eckstein M, Kollar M, Werner P (2009) Thermalization after an interaction quench in the Hubbard model. *Phys Rev Lett* 103:056403
9. Freericks JK, Krishnamurthy HR, Pruschke T (2009) Theoretical description of timeresolved photoemission spectroscopy: application to pump-probe experiments. *Phys Rev Lett* 102:136401

⁹ Another important aspect which was almost completely left out of our review is electron–phonon interactions, a topic which would in fact deserve a chapter of its own.

10. Dahlen NE, van Leeuwen R (2007) Solving the Kadanoff-Baym equations for inhomogeneous systems: application to atoms and molecules. *Phys Rev Lett* 98:153004
11. Kwong N-H, Bonitz M (2000) Real-time Kadanoff-Baym approach to plasma oscillations in a correlated electron gas. *Phys Rev Lett* 84:1768–1771
12. Abrikosov AA, Gorkov LP, Dzyaloshinskii IY (1965) Quantum field theoretical methods in statistical physics, vol 4, International series of monographs in natural philosophy. Pergamon Press, Oxford
13. Feynman RP (1949) The theory of positrons. *Phys Rev* 76:749–759
14. Dyson FJ (1949) The S matrix in quantum electrodynamics. *Phys Rev* 75:1736–1755
15. Wick GC (1950) The evaluation of the collision matrix. *Phys Rev* 80:268–272
16. Matsubara T (1955) A new approach to quantum-statistical mechanics. *Prog Theor Phys* 14 (4):351–378
17. Martin PC, Schwinger J (1959) Theory of many-particle systems. I. *Phys Rev* 115:1342–1373
18. Kadanoff LP, Baym G (1962) Quantum statistical mechanics, 1st edn. The Benjamin/Cumming Publishing Company Inc, Massachusetts
19. Konstantinov OV, Perel' VI (1961) Graphical technique for evaluation of kinetic quantities. *JETP* 12(142):142–149
20. Keldysh LV (1965) Diagram technique for nonequilibrium processes. *JETP* 20(4):1018–1026
21. Danielewicz P (1984) Quantum theory of nonequilibrium processes, I. *Ann Phys* 152 (2):239–304
22. Gell-Mann M, Low F (1951) Bound states in quantum field theory. *Phys Rev* 84:350–354
23. van Leeuwen R, Dahlen NE (2004) Conserving approximations in nonequilibrium green function and density functional theory. In: The electron liquid paradigm in condensed matter physics, vol. 157, pp 169–188
24. van Leeuwen R, Dahlen N, Stefanucci G, Almladh C-O, von Barth U (2006) Introduction to the Keldysh formalism. In: Marques M, Ullrich C, Nogueira F, Rubio A, Burke K, Gross EKV (eds) Time-dependent density functional theory, vol. 706 of lecture notes in physics. Springer, Berlin, Heidelberg, pp 33–59
25. Baym G, Kadanoff L (1961) Conservation laws and correlation functions. *Phys Rev* 124 (2):287–299
26. Baym G (1962) Self-consistent approximations in many-body systems. *Phys Rev* 127 (4):1391–1401
27. Nambu Y (1960) Quasi-particles and gauge invariance in the theory of superconductivity. *Phys Rev* 117(3):648–663
28. Puig von Friesen M, Verdozzi C, Almladh C-O (2009) Successes and failures of Kadanoff-Baym dynamics in Hubbard nanoclusters. *Phys Rev Lett* 103(17):176404
29. Stan A, Dahlen NE, van Leeuwen R (2009) Time propagation of the Kadanoff-Baym equations for inhomogeneous systems. *J Chem Phys* 130(22):224101
30. Puig von Friesen M, Verdozzi C, Almladh C-O (2010) Kadanoff-Baym dynamics of Hubbard clusters: performance of many-body schemes, correlation-induced damping and multiple steady and quasi-steady states. *Phys Rev B* 82(15):1–19
31. Langreth DC (1976) Linear and nonlinear electron transport in solids. Plenum, New York
32. Köhler H, Kwong N, Yousif HA (1999) A Fortran code for solving the Kadanoff-Baym equations for a homogeneous fermion system. *Comput Phys Commun* 123(1–3):123–142
33. Kubo R, Yokota M, Nakajima S (1957) Statistical-mechanical theory of irreversible processes. II. Response to thermal disturbance. *J Phys Soc Jpn* 12(11):1203–1211
34. Kubo R (1957) Statistical-mechanical theory of irreversible processes. I. General theory and simple applications to magnetic and conduction problems. *J Phys Soc Jpn* 12(6):570–586
35. Balzer K, Hermanns S, Bonitz M (2012) Electronic double excitations in quantum wells: solving the two-time Kadanoff-Baym equations. *Europhys Lett* 98(6):67002
36. Säkkinen N, Manninen M, van Leeuwen R (2012) The Kadanoff-Baym approach to double excitations in finite systems. *New J Phys* 14(1):013032
37. Balzer K, Bonitz M, van Leeuwen R, Stan A, Dahlen NE (2009) Nonequilibrium Green's function approach to strongly correlated few-electron quantum dots. *Phys Rev B* 79 (24):245306

38. Attaccalite C, Grüning M, Marini A (2011) Real-time approach to the optical properties of solids and nanostructures: time-dependent Bethe-Salpeter equation. *Phys Rev B* 84 (24):245110
39. Marini A (2013) Competition between the electronic and phonon-mediated scattering channels in the out-of-equilibrium carrier dynamics of semiconductors: an ab-initio approach. *J Phys Conf Ser* 427:012003
40. Hedin L (1965) New method for calculating the one-particle Green's function with application to the electron-gas problem. *Phys Rev* 139(3A):A796–A823
41. Lipavský P, Špička V, Velický B (1986) Generalized Kadanoff-Baym ansatz for deriving quantum transport equations. *Phys Rev B* 34(10):6933–6942
42. Haug H, Jauho A (2007) *Quantum kinetics in transport and optics of semiconductors*. Springer, Berlin, Heidelberg
43. Hubbard J (1963) Electron correlations in narrow energy bands. *Proc R Soc Lond* 276 (1365):238–257
44. Cini M, Verdozzi C (1987) Many-body effects in the electron spectroscopies of incompletely filled bands. *Nuovo Cimento D* 9(1):1–21
45. Verdozzi C, Godby R, Holloway S (1995) Evaluation of GW approximations for the self-energy of a Hubbard cluster. *Phys Rev Lett* 74(12):2327–2330
46. Romaniello P, Bechstedt F, Reining L (2012) Beyond the GW approximation: combining correlation channels. *Phys Rev B* 85(15):34–39
47. Holm B, von Barth U (1998) Fully self-consistent GW self-energy of the electron gas. *Phys Rev B* 57(4):2108–2117
48. Hohenberg P, Kohn W (1962) Inhomogeneous electron gas. *Phys Rev* 155:1964
49. Kohn W, Sham L (1965) Self-consistent equations including exchange and correlation effects. *Phys Rev* 140(4A):1133–1138
50. Runge E, Gross EKV (1984) Density-functional theory for time-dependent systems. *Phys Rev Lett* 52(12):997–1000
51. van Leeuwen R (1999) Mapping from densities to potentials in time-dependent density-functional theory. *Phys Rev Lett* 82(19):3863–3866
52. Dreizler R, Gross EKV (1990) *Density functional theory*. Springer, Berlin
53. Botti S, Schindlmayr A, Sole RD, Reining L (2007) Time-dependent density-functional theory for extended systems. *Rep Prog Phys* 70(3):357–407
54. Marques M, Maitra N, Nogueira F, Gross EKV, Rubio A (eds) (2012) *Fundamentals of time-dependent density functional theory*. Springer, Berlin
55. Ullrich CA (2012) *Time-dependent density-functional theory. Concepts and applications*. Oxford graduate texts, vol xiv. Oxford University Press, Oxford, p 526, sterling 45.00
56. Gunnarsson O, Schönhammer K (1986) Density-functional treatment of an exactly solvable semiconductor model. *Phys Rev Lett* 56(18):1968–1971
57. Schönhammer K, Gunnarsson O, Noack R (1995) Density-functional theory on a lattice: comparison with exact numerical results for a model with strongly correlated electrons. *Phys Rev B* 52(4):2504–2510
58. Lima N, Silva M, Oliveira L, Capelle K (2003) Density functionals not based on the electron gas: local-density approximation for a Luttinger liquid. *Phys Rev Lett* 90(14):146402
59. Verdozzi C (2008) Time-dependent density-functional theory and strongly correlated systems : insight from numerical studies. *Phys Rev Lett* 101(16):166401
60. Li W, Xianlong G, Kollath C, Polini M (2008) Collective excitations in one-dimensional ultracold Fermi gases: comparative study. *Phys Rev B* 78(19):1–9
61. Baer R (2008) On the mapping of time-dependent densities onto potentials in quantum mechanics. *J Chem Phys* 128(4):044103
62. Li Y, Ullrich CA (2008) Time-dependent v -representability on lattice systems. *J Chem Phys* 129(4):044105
63. Farzanehpour M, Tokatly I (2012) Time-dependent density functional theory on a lattice. *Phys Rev B* 86(12):125130

64. Capelle K, Campo VL (2013) Density functionals and model Hamiltonians: pillars of many particle physics. *Phys Rep* 528(3):91–159
65. Vettchinkina V, Kartsev A, Karlsson D, Verdozzi C (2013) Interacting fermions in one-dimensional disordered lattices: exploring localization and transport properties with lattice density-functional theories. *Phys Rev B* 87(11):115117
66. Karlsson D, Privitera A, Verdozzi C (2011) Time-dependent density-functional theory meets dynamical mean-field theory: real-time dynamics for the 3D Hubbard model. *Phys Rev Lett* 106(11):116401
67. Metzner W, Vollhardt D (1989) Correlated lattice fermions in $d = \infty$ dimensions. *Phys Rev Lett* 62(3):324–327
68. Georges A, Kotliar G, Krauth W, Rozenberg M (1996) Dynamical mean-field theory of strongly correlated fermion systems and the limit of infinite dimensions. *Rev Mod Phys* 68(1):13–125
69. Kotliar G, Vollhardt D (2004) Strongly correlated materials: insights from dynamical mean-field theory. *Phys Today* 57(3):53–59
70. Kozik E, Van Houcke K, Gull E, Pollet L, Prokof'ev N, Svistunov B, Troyer M (2010) Diagrammatic Monte Carlo for correlated fermions. *Europhys Lett* 90(1):10004
71. Verdozzi C, Karlsson D, Puig von Friesen M, Almladh C-O, von Barth U (2011) Some open questions in TDDFT: clues from lattice models and Kadanoff–Baym dynamics. *Chem Phys* 391(1):37–49
72. van Leeuwen R (1996) The Sham–Schlüter equation in time-dependent density-functional theory. *Phys Rev Lett* 76(19):3610–3613
73. von Barth U, Dahlen NE, van Leeuwen R, Stefanucci G (2005) Conserving approximations in time-dependent density functional theory. *Phys Rev B* 72(23):235109
74. Uimonen A-M, Koshravi E, Stan A, Stefanucci G, Kurth S, van Leeuwen R, Gross EKV (2011) Comparative study of many-body perturbation theory and time-dependent density functional theory in the out-of-equilibrium Anderson model. *Phys Rev B* 84(11):115103
75. Freericks JK (2008) Quenching Bloch oscillations in a strongly correlated material: nonequilibrium dynamical mean-field theory. *Phys Rev B* 77(7):075109
76. Schiro M (2010) Real-time dynamics in quantum impurity models with diagrammatic Monte Carlo. *Phys Rev B* 81(8):085126
77. Gull E, Millis AJ, Lichtenstein AJ, Rubtsov AN, Troyer M, Werner P (2011) Continuum-time Monte Carlo methods for quantum impurity models. *Rev Mod Phys* 83:349–404
78. Kartsev A, Karlsson D, Privitera A, Verdozzi C (2013) Three-dimensional dynamics of a fermionic Mott wedding-cake in clean and disordered optical lattices. *Sci Rep* 3:2570
79. Puig von Friesen M, Verdozzi C, Almladh C-O (2011) Can we always get the entanglement entropy from the Kadanoff–Baym equations? The case of the T-matrix approximation. *Europhys Lett* 95(2):27005
80. Malet F, Gori-Giorgi P (2012) Strong correlation in Kohn–Sham density functional theory. *Phys Rev Lett* 109(24):246402
81. Mirschink A, Seidl M, Gori-Giorgi P (2013) The derivative discontinuity in the strong-interaction limit of density functional theory. *Phys Rev Lett* 111(12):126402
82. Malet F, Mirschink A, Cremon JC, Reimann SM, Gori-Giorgi P (2013) Kohn–Sham density functional theory for quantum wires in arbitrary correlation regimes. *Phys Rev B* 87(11):115146
83. Fuks JI, Farzanehpour M, Tokatly IV, Appel H, Kurth S, Rubio A (2013) The time-dependent exchange-correlation functional for a Hubbard dimer: quantifying non-adiabatic effects. *Phys Rev A* 88(6):062512
84. Elliott PJ, Fuks JI, Rubio A, Maitra NT (2012) Universal dynamical steps in the exact time-dependent exchange-correlation potential. *Phys Rev Lett* 109(26):266404
85. Uimonen A-M, Stefanucci G, van Leeuwen RR (2014) Ultra-nonlocality in density functional theory for photo-emission spectroscopy. *J Chem Phys* 140(18):18A526

86. Turkowski V, Rahman TS (2014) Nonadiabatic time-dependent spin-density functional theory for strongly correlated systems. *J Phys Condens Matter* 26(2):022201
87. Hermanns S, Balzer K, Bonitz M (2013) Few-particle quantum dynamics-comparing nonequilibrium Green's functions with the generalized Kadanoff-Baym ansatz to density operator theory. *J Phys Conf Ser* 427:012008
88. Latini S, Perfetto E, Uimonen A-M, van Leeuwen RR, Stefanucci G (2014) Charge dynamics in molecular junctions: nonequilibrium Green's function approach made fast. *Phys Rev B* 89 (7):075306
89. Dirks A, Mikelsons K, Krishnamurthy HR, Freericks JK (2013) Simulation of inhomogeneous distributions of ultracold atoms in an optical lattice via a massively parallel implementation of nonequilibrium strong-coupling perturbation theory. arXiv:1309.5994